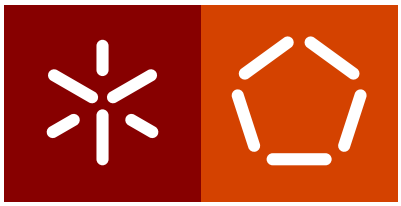

Universidade do Minho
Escola de Engenharia??
Departamento de Informática??

Jaime Santos

Quantum Random Walks
Second Part of Title

First Part of Subtitle
Second part of Subtitle

July 2021

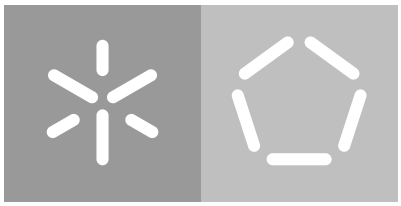

Universidade do Minho
Escola de Engenharia??
Departamento de Informática??

Jaime Santos

Quantum Random Walks
Second Part of Title

First Part of Subtitle
Second part of Subtitle

Master dissertation
Master Degree in Física da Informaçao

Dissertation supervised by
Luís Barbosa
Bruno Chagas

July 2021

ACKNOWLEDGEMENTS

Write acknowledgements here

ABSTRACT

Implementation of staggered quantum walks in qiskit. Testing github overleaf integration.

RESUMO

Pensar no que escrever aqui. Hello!

CONTENTS

LIST OF FIGURES

LIST OF TABLES

1

INTRODUCTION

1.1 BRIEF HISTORY OF QUANTUM COMPUTING

The modern understanding of computer science was firstly announced by Turing (1936) where he developed the abstract concept of what is now called a *Turing machine*. These machines are the mathematical foundation of programmable computers, and Turing showed that there is a *Universal Turing Machine* that can be used to simulate any other Turing Machine. This means that if an algorithm can be executed in any piece of hardware, then there is a Universal Turing Machine that can acompish the same task. This is known as the *Church-Turing thesis*, which connects the concept of what classes of algorithms can be run in some physical device with the mathematical framework of a Universal Turing Machine.

The paper published by Turing set in motion a series of events which led to the rapid advancement of eletronic computers and computer science. One of the earliest theoretical models developed by John von Neumann (work later published in von Neumann (1993)), presented how to assemble all the necessary parts to create a computer with all the capabilities of a Universal Turing Machine. The true explosion of innovation in this field came after the invention of the transistor in 1947 by John Bardeen and Walter Brattain. The creation of the transistor led to an unpredecent growth quantified by Moore (1965) where he created *Moore's law*, stating that computer power will double with constant cost approximately every two years. Moore's law has roughly held true throughout the decades, by the ever increasing miniaturization of the transistor technology. However, conventional fabrication methods run into a problem of scale, as quantum effects begin to interfere more as the size of the devices becomes smaller.

Feynman (1959) recognized such a miniturization was the way forward, and even predicted the problems quantum effects presented to a classical computer. With an amazing stroke of insight, Feynmann imagined that these effects could be exploited given the right computational paradigm. Quantum computing begins to take form in later work developed by Benioff (1980), where the earliest quantum mechanical model of a computer was described. In this paper, Benioff showed that a computer working under the laws of quantum mechanics could be used to express a Shrodinger equation description of Turing machines. Shortly

after, Feynman (1982) pointed out that simulating quantum systems on classical computers is inneficient, and suggested using quantum computers for this purpose. Additional work in the following decade further explored this idea and showed that there are systems that quantum computers can simulate, which have no known efficient simulation on a classical computer, and even today this continues to be one of the most promising fields in quantum computing.

Driven by the work of Turing, Deutsch (1985) questioned if a stronger version of the Church-Turing thesis could be derived from the laws of physics. The strong Church-Turing thesis states that any algorithmic process can be simulated efficiently using a probabilistic Turing machine, and Deutsh was set to define some device that could efficiently simulate an arbitrary physical system. Whether Deutsh's formulation of a Universal Quantum Computer is sufficient for this function is still an open question, but what he accomplished was a challenge to the strong Church-Turing thesis by suggesting that there are tasks a quantum computer can accomplish efficiently that a probabilistic Turing machine cannot. Deutsch and Jozsa (1992) present an example of a quantum algorithm that is exponentially faster than a classical counterpart, the *Deusth-Josza algorithm* that determines if a function is constant or balanced. Even though of little practical use, this is one of the first examples of possible advantages a quantum computer may have over a classical one.

Even though the Deutsh-Josza algorithm might not have real world applications, it led to further research on finding other such types of algorithms. Shor (1994a) showed that the problem of finding prime factors of an integer and the *discrete logarithm* problem can be effieciently solved by a quantum computer by an exponential factor. This brought a lot of interest to quantum computing, since both of these problems have real world applications and no efficient classical solution was/is known. Furthermore, most modern popular algorithms used for cryptography rely on the fact that the integer factorization or discrete logarithm problems are not effiently solvedi. Since this is no longer the case, a new field has emerged called *Post-quantum cryptography*, whose purpose is to find suitable classical algorithms for cryptography that are not efficiently solved by quantum computing.

A more modest, but very relevant advantage was presented by Grover (1996) where he presented a quantum algorithm that promised to speed up unstructured database searches quadratically. Even though it's not an exponential improvement like Shor's algorithm, search-based algorithms are useful in many contexts, so even a "small" quadratic gain generated a lot of interest.

Contemporary to computer science, information theory is another field very relevant to this topic. Shannon (1948) revolutionized how communication and information are understood. In his paper, Shannon was interested in defining what resources are requiried to send information over a communication channel and how to reliably send that information mitigating the effects of noise. This led to the creation of the two fundamental theorems of

information theory. Firstly, Shannon's *noiseless channel coding theorem* specifies what resources are needed to store information sent from a source. Secondly, the *noisy channel coding theorem*, specifies how much information can be sent through a channel subject to noise. Even though Shannon's second theorem does not define any specific methodology to reduce noise, it sets an upper limit on how much noise can be mitigated through said methodology. These are known as *error-correcting codes* and research has developed better and better codes that get closer and closer to Shannon's limit, and they are used wherever there is need to store or transmit information.

Similar progress was made in quantum information theory. Schumacher (1995) developed a quantum version of Shannon's noiseless coding theorem, where he defined a *quantum bit* as a physical resource. There is no analogue for the second Shannon theorem, but that didn't stop the development of quantum error-correcting theory. For example, Calderbank and Shor (1996) and Steane (1996) proposed an important class of quantum error-correcting codes known as CSS.

Error-correcting was designed to protect quantum states, but another discovery by Bennett and Wiesner (1992) showed another interesting aspect about quantum information when transmitting classical information through a quantum channel. They explained how to send two classical bits of information using only one qubit, in a phenomenon known as *superdense coding*.

Another interesting application of quantum information is in the field of cryptography. Wiesner (1983) showed how quantum mechanics could be used to make sure that a information sent could not be interfered with without destroying it. Building on this work, Bennett and Brassard (1984) proposed a quantum key distribution protocol between sender and receiver that could not spied upon without notice. Many other protocols have since been proposed and experimental prototypes developed.

Finally, another interesting field within quantum computation is based on the concept of *distributed quantum computation*. Quantum clusters show promise since they require exponentially less communication to solve certain problems, such as modeling quantum systems, but are stil in their infancy due to technical restrictions. There has been increasing international interest in taking advantage of these systems to build a *quantum internet* which promises better and safer transmission of information, but there are still many technological improvements to be made before this becomes a mainstream reality.

1.2 Classical and Quantum Random Walks

The strong Church-Turing thesis, that states that any algorithmic process can be simulated efficiently using a Turing Machine, was challenged by Solovay and Strassen (1977) where they presented what is known as the *Solovay-Strassen primality test*. They showed that it

is possible to test whether a integer is prime or composite using a randomized algorithm. The implication is that, because of the randomness, the Solvay-Strassen primality test does not determine with certainty whether a integer is prime or composite, rather it computes that a number is *probably* prime or else *certainly* composite. This is of significance since no deterministic test for primality was known at the time (nor it is now), meaning that this was an example of a class of problems that could not be efficiently solved by a conventional deterministic Turing Machine.

This led to a modification of the Church-Turing thesis, now stating that any algorithm can be simulated efficiently using a *probabilistic* Turing machine. The discovery of more instances of such algorithms followed, Motwani and Raghavan (1995) and Papadimitrious (1994) show several problems that can be solved based on randomized algorithms. For example, the *Quicksort* algorthim, developed by Hoare (1961), has a high probability of finishing in $O(n \log n)$. In contrast to many deterministic algorithms that require $O(n^2)$ time. They also show algorithms that take advantage of *Markov chains* and the *Monte Carlo method*. The volume of a convex body, proposed by Dyer et al. (1991), can be estimated by a randomized algorithm in polynomial time; the permanent of a nonnegative entry matrix can also be approximately calculated in probabilistic polynomial time as was shown by Jerrum et al. (2004) and the *k-SAT* and satisfiability with restrictions problem by Schöning (1999).

Random walks, as the name suggests, belong to this class of algorithms. Pearson (1905) coined the term random walk, and they can be described as path consisting of a succession of steps determined by a stochastic process, over a mathematical space. They are a special case of *Markov chains*, which are stochastic processes that assume discrete values and whose next state is dictated by a deterministic or random rule based only on the current state. This is a useful framework, since it can be used to explain the behaviour of systems across many fields, from the Brownian movement of particles moving through a gas, to the price of a fluctuating stock as shown by Cootner (1967).

The quantum analogue of the random walk was firstly developed by Aharonov et al. (1993), where they defined the *coined quantum random walk*. This model consists of a walker and a coin that determines the movement of the walker, which are both quantum systems where time is a discrete variable dictated by the successive quantum coin flips and shifts in position. Nayak and Vishwanath (2000) and Aharonov et al. (2001) presents the first analysis of the quantum walk on a graph described by a line. Further work by Inui et al. (2003) studies the behaviour of the walk on grids and Aharonov et al. (2001) on general regular graphs. The first algorithmic applications appear in the work of Shenvi et al. (2003) where they constructed a search problem based on the quantum random walk, and Ambainis (2007) applied it to the element distinction problem. On a more theoretical note, Konno (2002) demonstrated how the classical and quantum models of the random walk on the line differ, and Grimmett et al. (2003) generalized this to higher dimensions. Lovett

et al. (2010) demonstrated that any quantum algorithm can be reformulated as a discrete time quantum walk algorith, effectively showing that this model can be used for universal quantum computation.

A different model for quantum random walks emerged from the work of Farhi and Gutmann (1998), where a different way of computing a search problem was presented. They showed that evolving a system in time between an initial and final Hamiltonian is analogous to the Grover algorithm, but continuous in time. Farhi et al. (2000) revised their work, now known as an adiabatic evolution, to solve boolean *sat* problems. Childs and Goldstone (2004) formulated a model of a quantum walk in terms of adiabatic evolution, known as *continuous time quantum walk* or *adiabatic quantum walk*. Aharonov et al. (2007) showed that any quantum algorithm can be efficiently simulated using adiabatic evolution, meaning that it is polynomially equivalent to the conventional quantum computation model. Further work by Childs (2009) showed that this model is indeed universal. The main difference between these two quantum walk models relies on the fact that in the discrete case, the system evolves with the flipping of a coin and subsequent movement of the walker, whilst in the adiabatic case the system evolves smoothly in time.

Yet another way of thinking about quantum walks was announced by Szegedy (2004), where he describes a discrete model based on Markov chain random walks. At the foundation of this model is the duplication of a gaph, process by which a bipartite graph is created. Magniez et al. (2007) show how to use this walk for triangle detection in an undirected graph. Magniez et al. (2006) proposed a search problem, which takes advantage of ergodicity and simmetry properties of Markov chains, with quadratic gain compared to classical algorithms. Problems like element distinctness, matrix product verification and others were formulated within this framework by Santha (2008). Further work by Portugal (2015) established a connection between the coined and Szegedy's quantum walk, by defining a model that encompasses and expands the latter.

Patel et al. (2005) pointed that, at the time, there was confusion surrounding the scaling behaviour of discrete and adiabatic quantum walk algorithms. They argued that this was because the former model used a coin, which is an extra resource, and the latter didnt't. So, in an attempt to resolve this confusion, they showed that a discrete time quantum walk could be constructed without the use of a coin. A new way of thinking about quantum walks came with the development of the methods behind the construction of evolution operators, by Falk (2013), introducing the concept of*tesselations*, based on local diffusion operators. Portugal et al. (2015) studied this model applied to a line graph, using the tesselation idea to construct the evolution operators. Further work by Portugal et al. (2016) formalized this approach naming it *staggered quantum walk*, and showed instances where the Szegedy quantum walk is equivalent. This suggests that this is a more general model, being able to describe other discrete time quantum walks. Portugal et al. (2017) delved deeper into this

topic, adding Hamiltonians to the model, and Portugal and Fernandes (2017) shows how this can be instanced as a search problem in a grid. Finally, Coutinho and Portugal (2018) analyze how a continuous-time quantum walk can be casted into this discrete model and Moqadam et al. (2017) show a possible physical implementation of this walk.

1.3 State of the Art quantum walks implementations

One of the earliest works on a more computational approach to quantum random walks was by Marquezino and Portugal (2008), where they created a general simulator for discrete-time quantum walks on one- and two-dimensional lattices. They argued that this framework allowed reasearchers to focus more on the mathematical aspect of quantum walks, instead of the specific numerical implementations. Further work on these lattices was later presented by Sawerwain and Gielerak (2010), where they studied the simulation of quantum walks by taking advantage of the GPU and CUDA techonlogy. Another interesting program for simulating discre-time quantum walks came with the work of Berry et al. (2011). This package allows for direct simulation of these walks, and visualisation of the time-evolution on arbitrary undirected graphs. It also allowed for plotting of continuous-time quantum walks, provided the data was provided externally. There are, however, direct simulators of continuous-time quantum walks, the earliest being by Izaac and Wang (2015). Their distributed memory software claims to be able to perform efficient simulation of multi-particle continuous-time quantum walk based systems, on *High Performance Computing* platforms. Falloon et al. (2017) provide a *Mathematica* package that implements a simulator of *Quantum Stochastic Walks*, which are a generalization of the continuous-time model. These walks incorporate both coherent and incoherent dynamics, which means that quantum stochastic walks can be instantiated as both quantum walks and classical random walks. What this paper then provides is a way of implementing quantum walks on directed graphs, opening the door to applications ranging from the capture of energy by photosyntethic protein complexes, to page ranking algorithms used by search engines. This package was ported to and expanded in the *Julia* programming language by Glos et al. (2018).

In order to truly harness the power of quantum computing, however, one must be able to perform these algorithms on quantum hardware. For this purpous, various implementations of quantum walks on quantum circuits have been purposed. Douglas and Wang (2009) pioneered this approach by developing efficient quantum circuits for discrete-time quantum walks on highly symmetric graphs, whose resources scale logarithmically with the size of the state space. Shakeel (2020) presented a new approach for building circuits for the discrete model, reducing resource requirement by using the quantum Fourier transform. For the continuous-time quantum walk, work by Qiang et al. (2016) presents efficient quantum circuits for the circulant graph class, and also an experimental implementation on a

photonic quantum processor. In the same year, Loke and Wang (2017a) showed how to build continous-time quantum walk circuits for composite graphs, namely commuting graphs and Cartesian product of graphs. Considering the Szegedy quantum walk, Chiang et al. (2009) proposed an efficient method of creating quantum circuits for this model. In their work, they showed how to derive a quantum version of the arbitrary sparse classical random walk by approximating a *quantum update rule* with circuit complexity scaling linearly with the degree of sparseness of the structure. Loke and Wang (2017b) developed this method by showing that an efficient circuit for the Szegedy quantum walk can be constructed even if the structures are not sparse, given they posses translational symmetry in the columns of the transitional matrix. More specifically, they identified that the class of cyclic and bipartite graphs are compatible with this approach. Another interesting result in this paper was the creation of circuits that implement a quantum analogue of Google's *Page Rank* algorithm, in terms of Szegedy walks.

On the experimental side, there have been various implementations of quantum walks on quantum computers. On IBM's hardware, work by Balu et al. (2017) presents an efficient implementation of topological quantum walks where they ran the circuit on a five qubit computer over a 4 vertex lattice. Georgopoulos and Zuliani (2019) implements two instances of the discrete-time quantum walk. The first is based on the work of Douglas and Wang (2009) using generalized CNOT gates, and the second uses a rotational approach to the CNOT decomposition, which saves using an extra ancilla qubit register. They noted that IBM's simulator backend corresponded to the theoretical predictions, however the circuit for over three qubits was too much for the quantum hardware at that time. The paper presented by Shakeel (2020) also uses IBM's hardware to perform their formulation of the discrete-time quantum walk. For the staggered quantum walk model, work by Acasiete et al. (2020) obtains meaningful results when using the quantum computers to study the dynamics of this model on various graphs with 16 elements, requiring 4 qubits. They also modify these circuits to accomodate an oracle, showing that a spatial search algorithm could be performed on IBM's quantum computers for a search space of size 8, and with a bit of noise but still satisfactory for size 16.

1.4 Text overview and contributions

The motivation behind the contents in this dissertation is to create an expanded overview on the topic of quantum random walks. To better contextualize the rest of this thesis, chapter **??** presents the basic concepts and mathematical tools needed to study quantum walks.

Chapter 2 consists of the study of three major quantum random walk models, more specifically the discrete-time coined quantum walk, the continuous-time quantum walk and the staggered quantum walk. For each of these models, this work presents the theoretical

framework as well as Python implementations. In these simulations, the dynamics of the walks are analised by changing various parameters, plotting the resulting probability distributions and seeing how these parameters alter the shape, propagation and other features of the quantum random walks.

Chapter 3 follows this approach, but now the structure where these walks take place is a complete graph and the goal is to find a marked element. For this purpose, the section about Grover's algorithm is used to introduce the notion of quantum searching problems. The following sections show how to change the various models of quantum walks to accomodate an oracle, thus performing an element search in time similar to Grover's algorithm.

Finally, chapter 4 is dedicated to constructing circuits for the models previously defined, using IBM's software *Qiskit* and their hardware. The first three sections are used to create circuits for the dynamics of the walks. The biggest contribution being the circulant graph approach to building diagonal operators for the continuous-time quantum walk, which can be easily translated to Qiskit circuits. Although work by Qiang et al. (2016) pioneered this approach, the work presented in this thesis aims to give a clear description on how to build these circuits in Qiskit and an original analysis on how the approximate quantum Fourier transform affects the accuracy of the results and the number of operations needed to perform the quantum walk. The last section shows how introduce an oracle to the various circuits in order to perform a searching problem. For the continuous-time case, circulant graphs are again used in an original implementation of the searching problem making use of diagonal operators and the Suzuki-Trotter expansion.

2

QUANTUM WALKS

2.1 CLASSICAL RANDOM WALK

The term *random walk*, firstly introduced by Pearson (1905), is classically defined as a stochastic process that models the path a walker would take through a mathematical space, where each step made by the walker is random. This can be used to model systems such as a molecule displaying Brownian motion in a fluid, or even fluctuating stock prices as can be seen in Sottinen (2001).

The simplest instance of this walk is on an infinite discretely numbered line, whose mathmatical space is composed of integer numbers. Here, the walker can only advance with equal probability in one of two directions, depending on the outcome of a random event such as tossing a coin. Starting from position $x = 0$, the walker moves to $x = +1$ or $x = -1$ with $\frac{1}{2}$ probability after the first toss. On the second toss, the walker could be on $x = \pm 2$ with $\frac{1}{4}$ probability each, and on $x = 0$ with $\frac{1}{2}$. Continuing this trend will result in a normal probability distribution around the origin, as can be seen in the Python coding of figure 1.

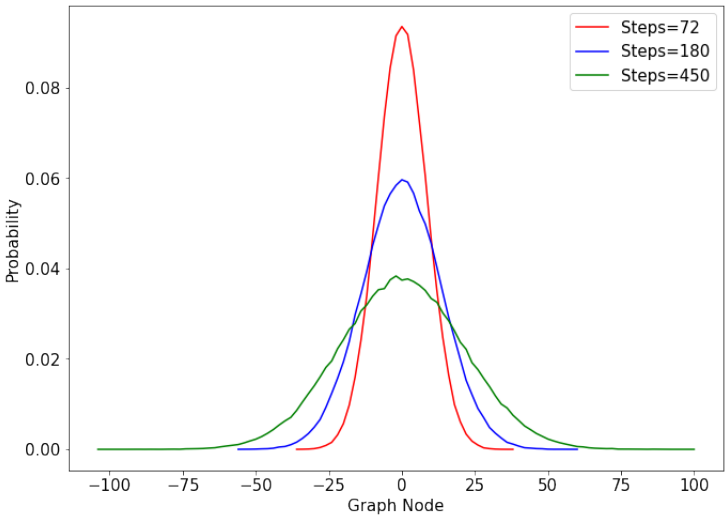

Figure 1: Classical Walk Temp.

The number of iterations directly affects how far the walker can reach. As the number of steps increases, the height of each curve at the starting position decreases and the width of the curve increases. This relationship can be captured by the *position standard deviation*, and Portugal (2018) shows that the standard deviation is

$$\sigma(t) = \sqrt{t}. \tag{1}$$

In other words, equation 1 represents the rate at which a walker moves away from the origin.

Note that this algorithm can be abstracted to graphs of higher dimensions. For example, in a two dimensional lattice, a walker would be transversing a plane with integer coordinatesi, choosing one of four directions in every intersection. Notably, Pólya (1921) proved that a walker in a two dimensional lattice will almost surely return to the origin at some point. However, the probability of returning to the origin decreases as the number of dimensions increases, as shown by Montroll (1956) and Finch (2003).

It is worth noting that a random walk, over a graph whose nodes are weighed and directed, is analagous to a *discrete-time Markov chain*[1].

The following sections will be used to describe various models of a quantum counterpart of the classical random walk.

2.2 COINED QUANTUM WALK

In the quantum case, the walker is a quantum system whose position on a discretely numbered line, is described by a vector $|x\rangle$ in Hilbert Space. The next position of the system will depend, in part, of a unitary operator, which can be viewed as a quantum coin. The analogy is, if the coin is tossed and rolls "heads", for example, the system transitions to position $|x+1\rangle$, otherwise it advances to $|x-1\rangle$. From a physical perspective, this coin can be the spin of an electron or the chirality of a particle, for example, and the outcome of measuring these properties decides whether the walker moves left or right. The coin is a unitary operator defined as

$$\begin{cases} C\,|0\rangle\,|x\rangle = a\,|0\rangle\,|x\rangle + b\,|1\rangle\,|x\rangle \\ C\,|1\rangle\,|x\rangle = c\,|0\rangle\,|x\rangle + d\,|1\rangle\,|x\rangle\,, \end{cases} \tag{2}$$

1 A Markov chain can be described as a sequence of stochastic events where the the probability of each event depends only on the state of the previous event.

where a, b, c and d are the amplitudes associated with each outcome of the coin toss. One of the most commonly used coins is the unbiased coin, also known as Hadamard operator

$$H = \begin{pmatrix} a & c \\ b & d \end{pmatrix} = \frac{1}{\sqrt{2}} \begin{pmatrix} 1 & 1 \\ 1 & -1 \end{pmatrix}, \tag{3}$$

which will be the one used in this example.

The Hilbert space of the system is $\mathscr{H} = \mathscr{H}_C \otimes \mathscr{H}_P$, where $\mathscr{H}_C$ is the two-dimensional Hilbert space associated with the coin and $\mathscr{H}_P$ is the Hilbert space of the walker.

The transition from $|x\rangle$ to either $|x+1\rangle$ or $|x-1\rangle$ must be described by a unitary operator, the *shift operator*

$$\begin{cases} \mathcal{S} |0\rangle |x\rangle = |0\rangle |x+1\rangle \\ \mathcal{S} |1\rangle |x\rangle = |1\rangle |x-1\rangle , \end{cases} \tag{4}$$

that can also be described by

$$S = |0\rangle \langle 0| \otimes \sum_{x=-\infty}^{x=\infty} |x+1\rangle \langle x| + |1\rangle \langle 1| \otimes \sum_{x=-\infty}^{x=\infty} |x-1\rangle \langle x| . \tag{5}$$

It follows that the operator that describes the dynamics of the quantum walk will be given by

$$U = S(C \otimes I) = S(H \otimes I). \tag{6}$$

Consider a quantum system located at $|x=0\rangle$ with coin state $|0\rangle$, for $t=0$. It's state will be described by

$$|\Psi(0)\rangle = |0\rangle |x=0\rangle . \tag{7}$$

After t steps

$$|\Psi(t)\rangle = U^t |\Psi(0)\rangle , \tag{8}$$

more explicitly

$$|\Psi(0)\rangle \xrightarrow{U} |\Psi(1)\rangle \xrightarrow{U} |\Psi(2)\rangle \xrightarrow{U} (...) \xrightarrow{U} |\Psi(t)\rangle . \tag{9}$$

In other words, the coined quantum walk algorithm consists on applying the coin operator followed by the shift operator a certain number of times. Iterating this twice, evolves the system to the following respective states

$$|\Psi(1)\rangle = \frac{|0\rangle |x=-1\rangle + |1\rangle |x=1\rangle}{\sqrt{2}} \tag{10}$$

$$|\Psi(2)\rangle = \frac{|0\rangle |x=-2\rangle + |1\rangle |x=0\rangle + |0\rangle |x=0\rangle - |1\rangle |x=2\rangle}{2} \tag{11}$$

$$\tag{12}$$

If one were to measure the system after the first application of $\mathcal{U}$, it would be expected to see the walker at $x = 1$ with probability $P(x) = \frac{1}{2}$, and at $x = -1$ with $P(x) = \frac{1}{2}$ aswell. Measure the system t times, after each application of $\mathcal{U}$, and the result is a binomial probability distribution similar to the one in 1. The conclusion is that repetitive measurement of a coined quantum walk system reduces to the classical case, which means that any desired quantum behaviour is lost.

It is possible, however, to make use of the quantum correlations between different positions to generate constructive or destructive interference, by applying the Hadamard and shift operators successively without intermediary measurements. The consequences of interference between states become very apparent after only 3 iterations

$$|\Psi(3)\rangle = \frac{|1\rangle\,|x=-3\rangle - |0\rangle\,|x=-1\rangle + 2(|0\rangle + |1\rangle)\,|x=1\rangle + |0\rangle\,|x=3\rangle}{2\sqrt{2}}. \tag{13}$$

Even though an unbiased coin was used, this state is not symmetric around the origin and the probability distributions will not be centered in the origin. Moreover, Portugal (2018) shows that the standard deviation will be

$$\sigma(t) \approx 0.54t. \tag{14}$$

This means that the standard deviation for the coined quantum walk grows linearly in time, unlike the classical case which grows with $\sqrt{t}$, as was seen in equation 1. The implication is that the quantum walk displays *ballistic* behaviour, as is reviewed in Venegas-Andraca (2012). This behaviour is usually defined in the context of a moving free particle with unit velocity in a single direction, which is expected to be found at $x = t$ after t steps. The velocity of a walker in a Hadamard quantum walk is approximately half of the free particle example, which is still a quadratic improvement over the classical random walk.

This quadratic gain implies exponentially faster hitting times in certain graphs, as shown by Childs et al. (2002), meaning improvements to problems that require transversing graphs. Ambainis (2007) also shows advantages of the coined quantum walk model in element distinctness problems, and Childs and Goldstone (2004) show advantages in spatial search problems, which will be studied in a later chapter.

In order to study this distribution, a simulation of the coined quantum walk was coded in *Python*. Figure 2 is the result of using the Hadamard coin and the initial condition in equation 7, for varying numbers of steps. Analyzing the plot, it is noticeable that the distributions are asymmetric. The probability of finding the walker on the right-hand side is much larger than on the left, with a peak around $x \approx \frac{t}{\sqrt{2}}$. Regardless of number of steps, this peak is always present (albeit in varying positions), which is to say that the walker can always be found moving in a uniform fashion away from the origin, consistent with ballistic behaviour.

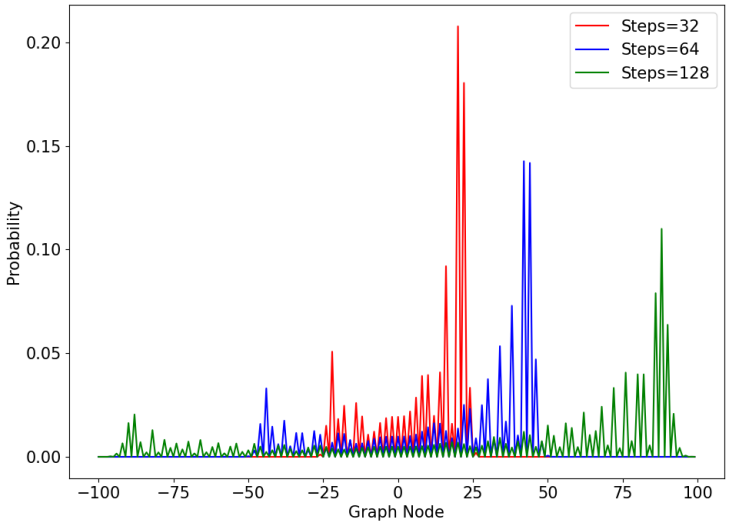

Figure 2: Probability distribution for the coined quantum walk on a line, after 100 steps, with initial condition $|\Psi(0)\rangle = |0\rangle\,|x=0\rangle$ and the Hadamard coin.

Another interesting case study is to find if this behaviour is preserved for a symmetric distribution around the origin. For this purpose, one must first understand where the asymmetry comes from. The Hadamard operator flips the sign of state $|1\rangle$, hence more

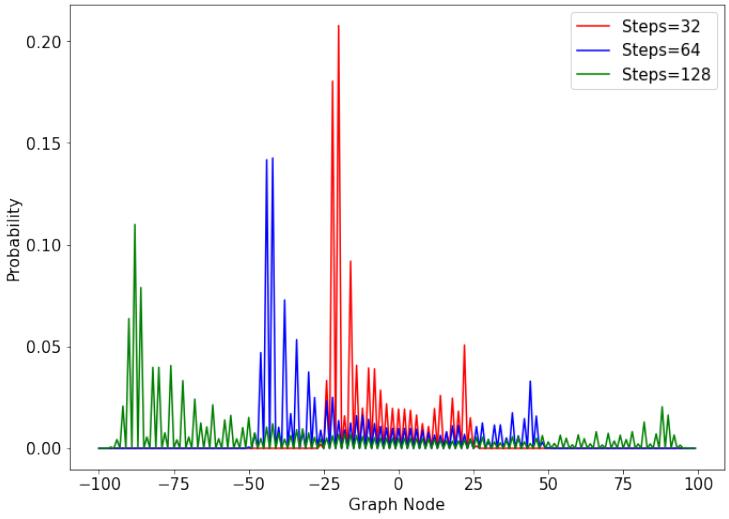

Figure 3: Probability distribution for the coined quantum walk on a line, after 100 steps, with initial condition $|\Psi(0)\rangle = -|1\rangle\,|x=0\rangle$ and the Hadamard coin.

terms are cancelled when the coin state is $|1\rangle$. Since $|0\rangle$ was defined to induce movement

to the right, the result is as shown in 2. Following this logic, it would be expected that an initial condition

$$|\Psi(0)\rangle = |1\rangle\,|x=0\rangle\,, \tag{15}$$

would result in more cancellations when the coin state is $|0\rangle$, thus the walker would be more likely found in the left-hand side of the graph. This is indeed what happens, as figure 3 is a mirror image of figure 2. The walker still moves away from the origin with ballistic behaviour, but in opposite direction. The peaks behave in a similar fashion, being instead found at $x \approx -\frac{t}{\sqrt{2}}$.

In order to obtain a symmetrical distribution, one must superpose the state in equation 7 with the state in equation 15. However, in order to not cancel terms before the calculation of the probability distribution, one must multiply state $|1\rangle$ with the imaginary unit, i

$$|\Psi(0)\rangle = \frac{|0\rangle + i\,|1\rangle}{\sqrt{2}}\,|x=0\rangle\,. \tag{16}$$

This works because the entries of the Hadamard operator are real numbers. Terms with the imaginary unit will not cancel out with terms without it, thus the walk can proceed to both left and right, as it is shown in figure 4.

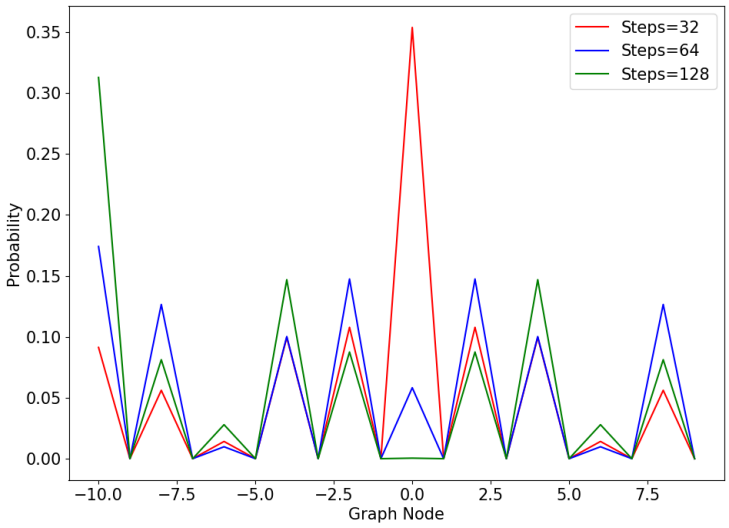

Figure 4: Probability distribution for the coined quantum walk on a line, after 100 steps, with initial condition $|\Psi(0)\rangle = \frac{|0\rangle - i|1\rangle}{\sqrt{2}}\,|x=0\rangle$ and the Hadamard coin.

The probability distribution is now symmetric and it is spread over the range $[-\frac{t}{\sqrt{2}}, -\frac{t}{\sqrt{2}}]$ with peaks around $x \approx \pm\frac{t}{\sqrt{2}}$. This means that if the position of the walker was measured at

the end, it would be equally probable to find him either in the left side or the right side of the graph , which is not possible in a classical diffusive motion.

All of the previous examples are in sharp contrast with the classical random walk distribution in figure 1. There, maximum probability is reached at $x = 0$ since there are approximately equal steps in both directions. Furthermore, the further the vertex is away from the origin, the less likely the walker is to be found there. However, in the quantum case, the walker is more likely to be found away from the origin as the number of steps increases. More specifically, the walk spreads quadratically faster than the classical counterpart.

This is but one model of a quantum random walk. As it will be seen in further sections, there are other approaches to creating both discrete and continuous quantum walk models that do not use a coin.

2.3 STAGGERED QUANTUM WALK

Similarly to the continuous-time quantum walk, the staggered case aims to spread a transition probability to neighboring vertices but with discrete time steps. The notion of adjacency now comes from cliques[2], and the initial stage of this walk consists in partitioning the graph in several different cliques. This is called tessellation, and it is defined as the division of the set of vertices into disjoint cliques. An element of a tessellation $\mathscr{T}$ is called a polygon, and it's only valid if if all of its vertices belong to the clique in $\mathscr{T}$. The set of polygons of each tessellation must cover all vertices of the graph, and the set of tessellations ($\mathscr{T}_1$,$\mathscr{T}_2$,...,$\mathscr{T}_k$) must cover all edges.

These definitions allow the construction of operators H_1,H_2,...,H_k that will be used to propagate the probability amplitude locally, in each polygon. The state associated to each polygon is

$$\left|u_j^k\right\rangle = \frac{1}{\sqrt{\left|\alpha_j^k\right|}} \sum_{l \in \alpha_j^k} |l\rangle \tag{17}$$

where α_j^k is the $j-th$ polygon in the $k-th$ tessellation.

The unitary and Hermitian operator H_k, associated to each tessellation is defined in Portugal et al. (2017) as

$$H_k = 2 \sum_{j=1}^{p} \left|u_j^k\right\rangle \left\langle u_j^k\right| - I \tag{18}$$

Solving the time-independent Schrodinger equation for this Hamiltonian gives the evolution operator

$$U = e^{i\theta_k H_k} ... e^{i\theta_2 H_2} e^{i\theta_1 H_1} \tag{19}$$

2 A clique is defined as the subset of vertices of an undirected graph such that every two distinct vertices in each clique are adjacent.

where

$$e^{i\theta_k H_k} = \cos(\theta_k) I + i \sin(\theta_k) H_k \tag{20}$$

since $H_k^2 = I$.

The simplest use case of this quantum walk model is the one-dimensional lattice, where the minimum tessalations are

$$\mathscr{T}_\alpha = \{\{2x, 2x+1\} : x \in \mathbb{Z}\} \tag{21}$$

$$\mathscr{T}_\beta = \{\{2x+1, 2x+2\} : x \in \mathbb{Z}\} \tag{22}$$

Each element of the tessellation has a corresponding state, and the uniform superposition of these states is

$$|\alpha_x\rangle = \frac{|2x\rangle + |2x+1\rangle}{\sqrt{2}} \tag{23}$$

$$|\beta_x\rangle = \frac{|2x+1\rangle + |2x+2\rangle}{\sqrt{2}} \tag{24}$$

One can now define Hamiltonians H_α and H_β as

$$H_\alpha = 2 \sum_{x=-\infty}^{+\infty} |\alpha_x\rangle \langle\alpha_x| - I \tag{25}$$

$$H_\beta = 2 \sum_{x=-\infty}^{+\infty} |\beta_x\rangle \langle\beta_x| - I \tag{26}$$

The Hamiltonian evolution operator reduces to

$$U = e^{i\theta H_\beta} e^{i\theta H_\alpha} \tag{27}$$

and applying it to an initial condition $|\Psi(0)\rangle$ results in the time evolution operator

$$U |\Psi(t)\rangle = U^t |\Psi(0)\rangle \tag{28}$$

Having defined the time evolution operator, the walk is ready to be coded with a certain initial condition and θ value, to better understand how the probability distribution spreads through time.

For the first case study, the initial condition will be a uniform superposition of states $|0\rangle$ and $|1\rangle$ and the θ value will be varied in order to understand how this parameter impacts the walk

The overall structure of the probability distribution remains the same, the difference is that the walker is more likely to be found further away from the origin as the angle increases.

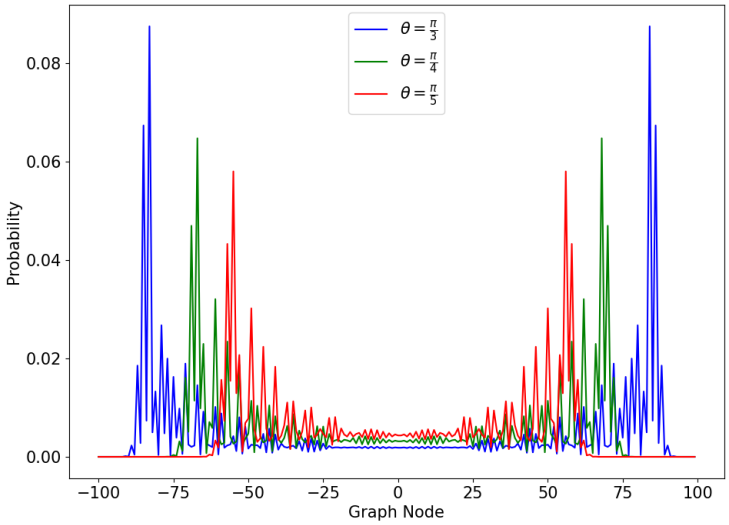

Figure 5: Probability distribution for the staggered quantum walk on a line after 50 steps, with initial condition $|\Psi(0)\rangle = \frac{|0\rangle+|1\rangle}{\sqrt{2}}$, for multiple angles.

Another interesting case study is to see how the initial condition affects the dynamics of the system

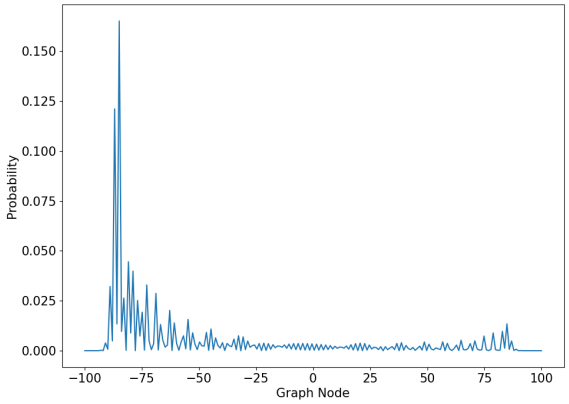

Figure 6: $|\Psi(0)\rangle = |0\rangle$

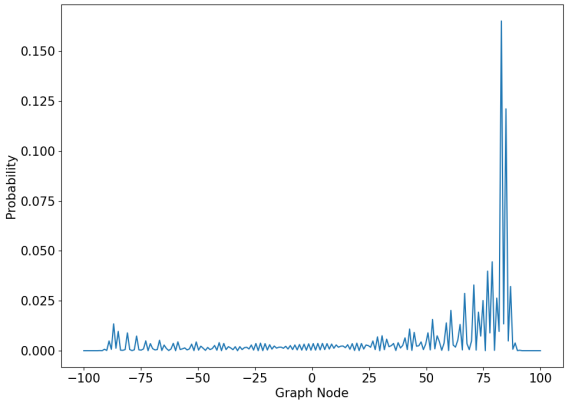

Figure 7: $|\Psi(0)\rangle = |1\rangle$

Similarly to the coined case, each initial condition results in asymmetric probability distributions, $|\Psi(0)\rangle = |0\rangle$ leads to a peak in the left-hand side while condition $|\Psi(0)\rangle = |1\rangle$ results in a peak in the right-hand side. As was shown in **??**, the uniform superposition of both these conditions results in a symmetric probability distribution.

2.4 CONTINUOUS-TIME QUANTUM WALK

The continuous-time random walk model on a graph is a Markov process where transitions have a fixed probability per unit time γ of moving to adjacent vertices, firstly introduced by Montroll and Weiss (1997). Consider a graph G with N vertices and no self-loops, this walk can be defined by the linear differential equation that describes the probability of jumping to a connected vertex in any given time

$$\frac{dp_i(t)}{dt} = \gamma \sum_j L_{ij} p_j(t), \tag{29}$$

where L is the Laplacian defined as $L = A - D$. A is the adjacency matrix that represents each vertex connection, given by

$$A_{ij} = \begin{cases} 1, & \text{if } (i,j) \in G \\ 0, & \text{otherwise,} \end{cases} \tag{30}$$

and D is the diagonal matrix $D_{jj} = deg(j)$ corresponding to the degree[3] of a vertex j.

In the quantum case, the nodes are quantum states that form the basis for the Hilbert space. The continuous-time quantum walk model will also be described by a differential equation, the Schrödinger equation

$$i\hbar \frac{d\,|\Psi(t)\rangle}{dt} = \hat{H}\,|\Psi(t)\rangle\,, \tag{31}$$

where $\hat{H} = -\gamma L$ is the Hamiltonian of the system. More explicitly,

$$\hat{H}_{ij} = \begin{cases} deg(j)\gamma, & \text{if } i = j; \\ -\gamma, & \text{if } i \neq j \text{ and adjacent;} \\ 0, & \text{if } i \neq j \text{ and not adjacent.} \end{cases} . \tag{32}$$

A general state of a system $|\Psi(t)\rangle$ can be written as a function of it's complex amplitudes

$$q_i = \langle i|\Psi(t)|i|\Psi(t)\rangle\,, \tag{33}$$

which means 31 can be rewritten as

$$i\hbar \frac{dq_i(t)}{dt} = \sum_j \hat{H}_{ij} q_j(t). \tag{34}$$

3 The degree of a vertex refers to the number of edges that it is connected to.

This highlights the similarities between the Schrödinger equation and 29. One of the main differences is the complex phase i, which will result in a very different behaviour. Setting $\hbar = 1$ and solving the differential equation results in the evolution operator of this walk

$$U(t) = e^{-iHt} = e^{i(-\gamma L)t} = e^{-i\gamma(A+D)t} \tag{35}$$

In the regular graph case, where D is simply the degree of the whole graph multiplied by the identity matrix, A and D will commute, meaning that the evolution operator can be written in terms of the adjacency matrix

$$U(t) = e^{-i\gamma At + i\gamma Dt} = e^{-i\gamma At} e^{i\gamma Dt} = \phi(t) e^{-i\gamma At} \tag{36}$$

since the degree matrix becomes a global phase. Applying this operator to an initial condition $\Psi(0)$, will give the state of the system at a time t

$$|\Psi(t)\rangle = U(t) \, |\Psi(0)\rangle \, . \tag{37}$$

Considering a uni-dimensional quantum system, each vertex will have at most 2 other neighboring vertices, reducing equation 32 to

$$\hat{H}_{ij} = \begin{cases} 2\gamma, & \text{if } i = j; \\ -\gamma, & \text{if } i \neq j \text{ and adjacent;} \\ 0, & \text{if } i \neq j \text{ and not adjacent.} \end{cases} \tag{38}$$

For a more detailed visualization, this quantum walk model was coded in python and figure 8 was obtained setting the transition rate to $\gamma = \frac{1}{2\sqrt{2}}$ the initial condition to $|\Psi(0)\rangle = |0\rangle$

A brief look at figure 8 reveals several similarities to the coined quantum walk model of figure **??**. Both have two peaks away from the origin and low probability near the origin. However, in the previous quantum walk, these characteristics were altered as a function of the chosen coin and initial condition, whereas in this case different values of γ will influence the probability distribution. For example, a lower value of γ will limit the spread of the probability distribution, as is shown in figure 10.

Moreover, the effects of altering the initial condition will also differ in the continuous-time example. For example, setting the initial condition to the balanced superposition of states $|0\rangle$ and $|1\rangle$ has no effect on the overall pattern of the probability distribution as can be seen in figure 12. Both peaks still are still present and at the same distance from the origin, with intermediate amplitudes being attenuated relative to figure 8. This behaviour is in contrast with the discrete-time case, where a change in the initial condition would dictate the number of peaks and where they would appear.

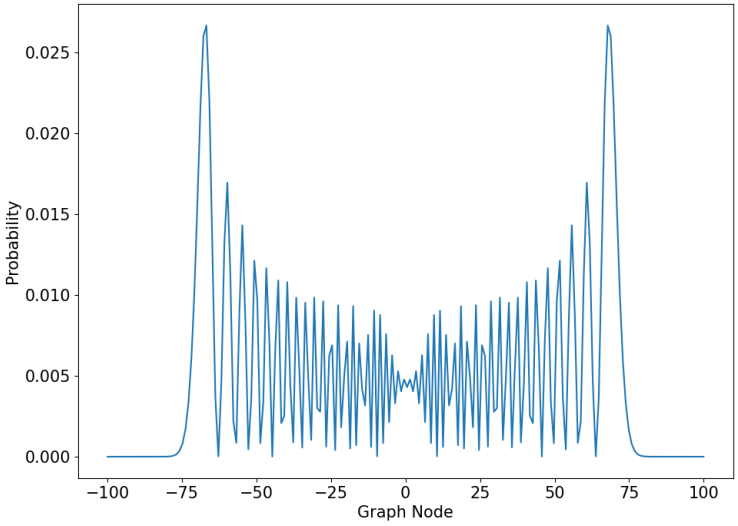

Figure 8: Probability distribution for the continuous-time quantum walk on a line, at t = 100, with initial condition $|\Psi(0)\rangle = |0\rangle$ and $\gamma = \frac{1}{2\sqrt{2}}$.

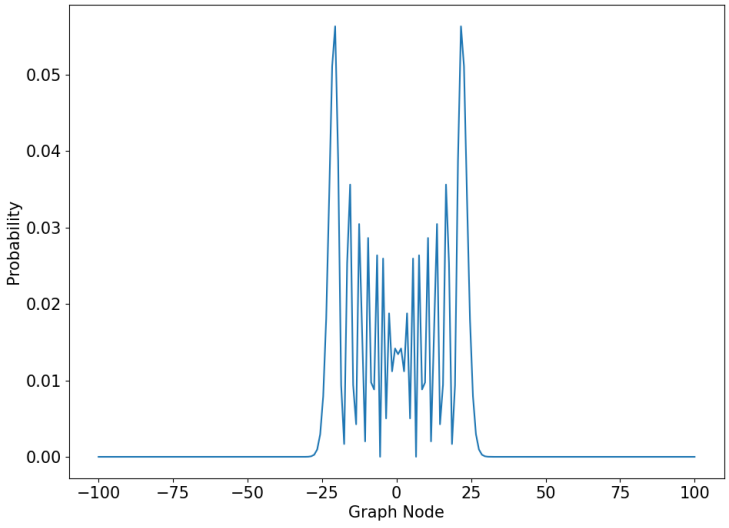

Figure 9: Probability distribution for the continuous-time quantum walk on a line, after 100 steps, with initial condition $|\Psi(0)\rangle = |0\rangle$ and $\gamma = \frac{1}{6\sqrt{2}}$.

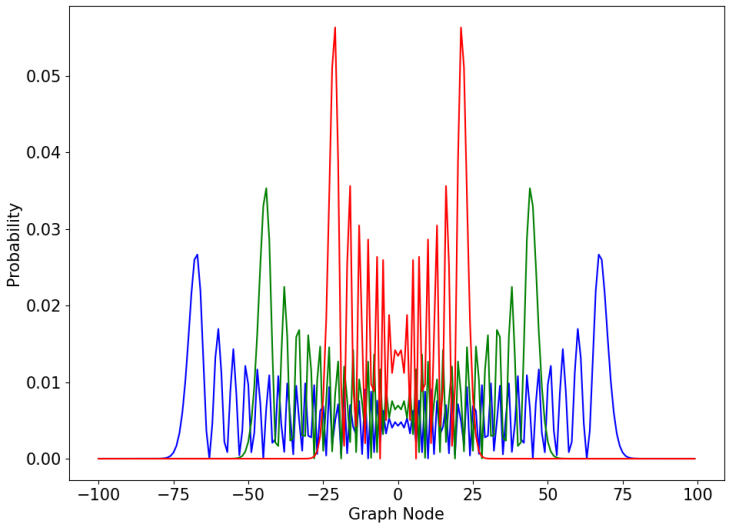

Figure 10: Temporary

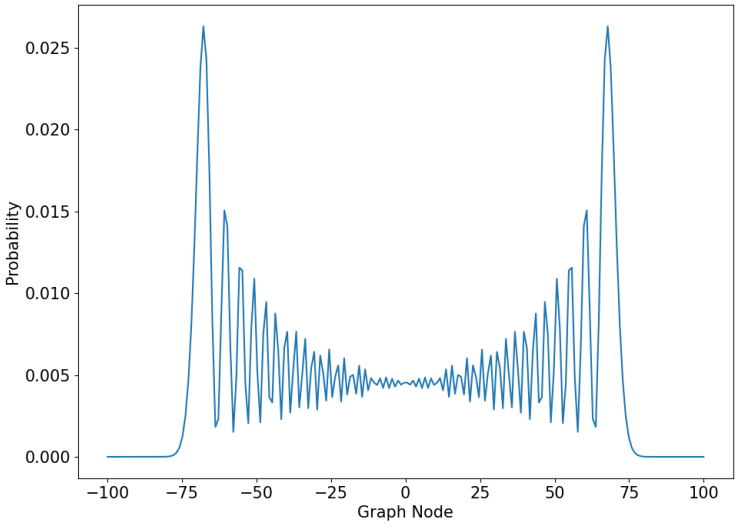

Figure 11: Probability distribution for the continuous-time quantum walk on a line, after 100 steps, with initial condition $|\Psi(0)\rangle = \frac{|0\rangle+|1\rangle}{\sqrt{2}}$ and $\gamma = \frac{1}{2\sqrt{2}}$.

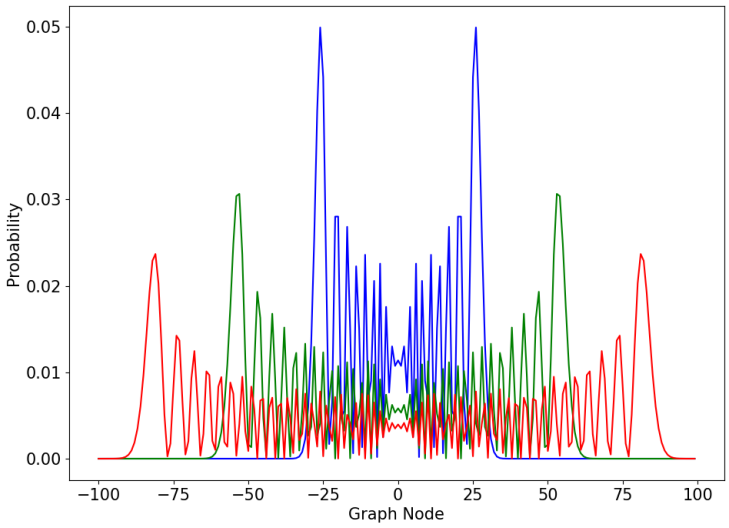

Figure 12: Temporary

3

SEARCHING PROBLEMS

3.1 GROVER'S ALGORITHM

Searching through an unstructured database is a task classically achieved by exhaustively evaluating every element in the database. Assume there exists a black box (oracle) that can be asked to find out if two elements are equal. Since we're looking for a specific element in a database of size N, we'd have to query the oracle on average $\frac{N}{2}$ times, or in the worst case N times.

Grover's algorithm, presented in Grover (1996), comes as a quantum alternative to this type of problems, taking advantage of superposition by increasing desirable states' amplitudes through a process called *amplitude amplification*. This method has a quadratic gain over the classical counterpart Boyer et al. (1998), being able to find a target element in expected time $\mathcal{O}(\sqrt{N})$.

Let us now expand on the inner workings of the black box. We start by focusing on searching indexes instead of directly evaluating the element and we assume $N = 2^n$, n being a positive integer. We can now define a function $f : \{0, 1, ..., N-1\}$ that returns 1 when evaluating the desired (marked) element and 0 otherwise. Since this function is to be applied to a quantum system, we must build a unitary operator $\mathcal{O}$

$$\mathcal{O} |x\rangle |i\rangle = |x\rangle |i \oplus f(x)\rangle . \tag{39}$$

where $|x\rangle$ is the index register, $\oplus$ is the binary sum operation and $|i\rangle$ is a qubit that is flipped if $f(x) = 1$.

The action of the oracle on state $|0\rangle$ will be

$$\mathcal{O} |x\rangle |0\rangle = \begin{cases} |x_0\rangle |1\rangle , & \text{if } x = x_0 \\ |x\rangle |0\rangle , & \text{otherwise.} \end{cases} \tag{40}$$

where x_0 is the marked element. More generically, $\mathcal{O}$ can be written as

$$\mathcal{O}|x\rangle = (-1)^{f(x)}|x\rangle . \tag{41}$$

This offers a bit of insight into the oracle, it *marks* the solutions to the search problem by applying a phase shift to the solutions. The question now is, what is the procedure that determines a solution x_0 using $\mathcal{O}$ the minimum number of times? The answer lies in the amplitude amplification section of Grover's search, starting with the creation of a uniform superposition

$$|\Psi_0\rangle = H^{\otimes n}|x\rangle = \frac{1}{\sqrt{N}}\sum_{x=0}^{N-1}|x\rangle \tag{42}$$

where $H^{\otimes n}$ is the *Hadamard* operator applied to an arbitrary number of states.

If we were to measure $|x\rangle$ at this point, the superposition would collapse to any of the base states with the same probability $\frac{1}{N} = \frac{1}{2^n}$, which means that on average, we'd need to try $N = 2^n$ times to guess the correct item. This is where amplitude amplification comes into effect, by means of a second unitary operator

$$\mathcal{D} = (2|\Psi_0\rangle\langle\Psi_0| - I) = H^{\otimes n}(2|0\rangle\langle 0| - I)H^{\otimes n} \tag{43}$$

This operator applies a conditional phase shift, with every computational basis state except $|0\rangle$ receiving a phase shift. This can also be described as the *inversion about the mean*, for a state of arbitrary amplitudes

$$|\phi\rangle = \sum_{k=0}^{N-1}\alpha_k|k\rangle \tag{44}$$

the action of $\mathcal{D}$ on state ϕ will be

$$\mathcal{D}|\phi\rangle = \sum_{k=0}^{N-1}(-\alpha_k + 2\langle\alpha\rangle)|k\rangle \tag{45}$$

where $\langle\alpha\rangle$ is the average of α_k

$$\langle\alpha\rangle = \frac{1}{N}\sum_{k=0}^{N-1}\alpha_k|k\rangle \tag{46}$$

The evolution operator that performs one step of the algorithm is then

$$\mathcal{U} = \mathcal{D}\mathcal{O} \tag{47}$$

and after t steps the state of the system is

$$|\Psi(t)\rangle = \mathcal{U}^t|\Psi_0\rangle . \tag{48}$$

3.1.1 *One marked element*

The optimal number of steps is, as aforementioned, proportional to $\sqrt{N}$. More precisely, if there's only one solution, maximum probability can be reached in *approximately* $\frac{\pi}{4}\sqrt{N}$ iterations. In order to show that this is the case, an iteration will be formally defined here as the process that transforms the state

$$|\Psi(k,l)\rangle = k\,|i_0\rangle + \sum_{i\neq i_0} l\,|i\rangle \tag{49}$$

into state $\left|\Psi(\frac{N-2}{N}k + \frac{2(N-1)}{N}l, \frac{N-2}{N}l - \frac{2}{N}k)\right\rangle$. Amplitudes l and k are real numbers that statisfy $k^2 + (N-1)l^2 = 1$. Running m iterations over state $|\Psi_0\rangle$ will eventually lead to state $|\Psi_j\rangle = |\Psi(k_j, l_j)\rangle$ after the $j-th$ iteration, where $k_0 = l_0 = \frac{1}{\sqrt{N}}$ and

$$\begin{cases} k_{j+1} = \frac{N-2}{N}k_j + \frac{2(N-1)}{N}l_j \\ l_{j+1} = \frac{N-2}{N}l_j + \frac{2}{N}k_j. \end{cases} \tag{50}$$

After the last iteration, the system will be in state $|\Psi_m\rangle$ with a certain amplitude. If that amplitude corresponds to the marked element x_0, then it is said that the algorithm was successful.

Grover (1996) proves that there exists a value of $m < \sqrt{2N}$ such that the probability of success is at least $\frac{1}{2}$. However the probability of success does not linearly increase with the number of iterations, in fact for $m = \sqrt{2N}$ the system will succeed less that 1 in 10 times. Boyer et al. (1998) argues that an explicit value of m is needed, and it is achieved by finding a closed form formula for k_j and l_j. The first step is to define an angle θ so that $\sin^2\theta = \frac{1}{N}$, and equation 50 will become

$$\begin{cases} k_{j+1} = \sin\left((2j+1)\theta\right) \\ l_{j+1} = \frac{1}{\sqrt{N-1}}\cos\left((2j+1)\theta\right). \end{cases} \tag{51}$$

In order to maximize the probability of success, one must find a value of m so that $k_m = 1$ and l_m is as close to 0 as possible. The value of k after m iterations will be at it's maximum when $\sin\left((2m+1)\theta\right) = \frac{\pi}{2}$, and solving the trigonometric equation leads to a value of $m = \frac{\pi - 2\theta}{4\theta}$. Conversely, $l_{\widetilde{m}} = 0$ when $\widetilde{m} = \frac{\pi-2\theta}{4\theta}$ for an integer number of $\widetilde{m}$. Setting m to the nearest lower integer of $\frac{\pi}{4\theta}$ will lead to

$$|m - \widetilde{m}| \leq \frac{1}{2} \iff |(2m+1)\theta - (2\widetilde{m}-1)\theta| \leq \frac{\pi}{2}. \tag{52}$$

By definition, $(2\widetilde{m}+1)\theta = \frac{\pi}{2}$ which means that $|\cos((2m+1)\theta)| \leq |\sin\theta|$. The probability of failure after m iterations can then be written as

$$(N-1)l_m^2 = \cos^2((2m+1)\theta) \leq \sin^2\theta = \frac{1}{N}. \tag{53}$$

Failure decreases as the number of elements increases. The run time of the algorithm will be

$$m \leq \frac{\pi}{4\theta} \leq \frac{\pi}{4}\sqrt{N} \tag{54}$$

since $\theta \geq \sin\theta = \frac{1}{\sqrt{N}}$. This means that, for a large N, the number of iterations that maximizes the probability of success will be very close to $\frac{\pi}{4}\sqrt{N}$.

Figure 13 was obtained by coding the apropriate operators as to simulate the system presented in equation 48. The unitary evolution operator was applied approximately

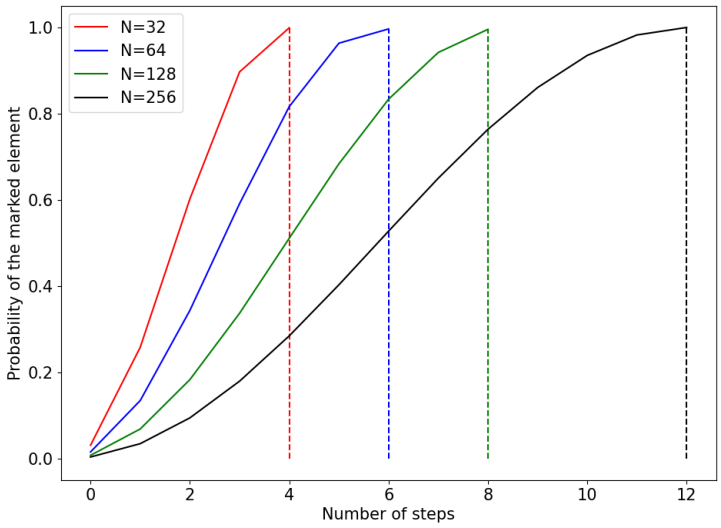

Figure 13: Grover one marked element temp.

$\frac{\pi}{4}\sqrt{N}$ times and the amplitudes associated with those states were stored as a probability distribution. Filtering the probability of the marked element and plotting it against the number of steps, shows that the maximum is indeed reached after the said number of iterations. It also shows that the maximum probability for $N = 16$ is lower than for $N = 128$, which makes sense since the the probability of success is maximized for larger values of N.

3.1.2 *Multiple marked elements*

When there's more than one element marked by the oracle, the number of iterations to achieve maximum probability changes. In fact, the latter part of this section will be used to discuss the case where one single iteration of this algorithm is enough to achieve maximum probability.

Firstly, one must define a set A that is composed of all the marked elements and set B of the remaining. The state from equation 49 will become

$$|\Psi(k,l)\rangle = \sum_{i\in A} k\,|i\rangle + \sum_{x\in B} l\,|x\rangle\,. \tag{55}$$

Assuming t marked elements, iterating over this state will result in

$$\left|\Psi\left(\frac{N-2t}{N}k + \frac{2(N-1)}{N}l, \frac{N-2}{N}l - \frac{2}{N}k\right)\right\rangle. \tag{56}$$

Choosing an angle θ such that $sin^2\theta = \frac{t}{N}$, allows the definition of the amplitudes associated with the states after j iterations

$$\begin{cases} k_j = \frac{1}{\sqrt{t}}\sin\left((2j+1)\theta\right) \\ l_j = \frac{1}{\sqrt{N-t}}\cos\left((2j+1)\theta\right). \end{cases} \tag{57}$$

Similarly to the one solution case, it can be shown that setting the number of iterations

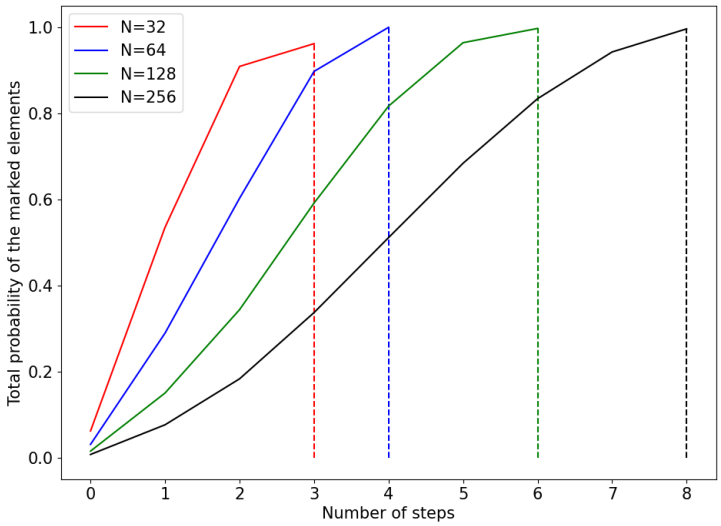

Figure 14: Grover Multiple marked temp.

m, to the nearest lower integer of $\frac{\pi}{4\theta}$ will result in a probability of failure $(N-t)l_m^2 \leq \frac{t}{N}$. Because $\theta \geq \sin\theta = \sqrt{\frac{t}{N}}$ then

$$m \leq \frac{\pi}{4\theta} \leq \frac{\pi}{4}\sqrt{\frac{N}{t}}. \tag{58}$$

From a more practical perspective, if one were to mark two elements of a 64 element set, maximum probability is expected to be reached in approximately 4 steps, since $\lfloor \frac{\pi}{4}\sqrt{\frac{64}{2}} \rfloor = 4$. Likewise, for $N = 256$, the number of iterations is rounded to 8, which is plotted along several other values of N in figure 14. The y-axis is now the sum total probability of the marked elements and the x-axis represents the range of steps that spans from 0 to $\lfloor \frac{\pi}{4}\sqrt{\frac{N}{2}} \rfloor$ for each N. Again, the probability of success approaches 1 as N increases. However, comparing to figure 13, the number of iterations that maximize probability is lower for each N, in agreement with equation 58.

3.1.3 *Single-Shot Grover*

An interesting case arises when the number of marked elements is set to $t = \frac{N}{4}$, because

$$sin^2\theta = \frac{\frac{N}{4}}{N} = \frac{1}{4} \iff \sin\theta = \frac{1}{2} \iff \theta = \frac{\pi}{6}. \tag{59}$$

Note that there are an infinite number of negative and positive solutions, but equation 59

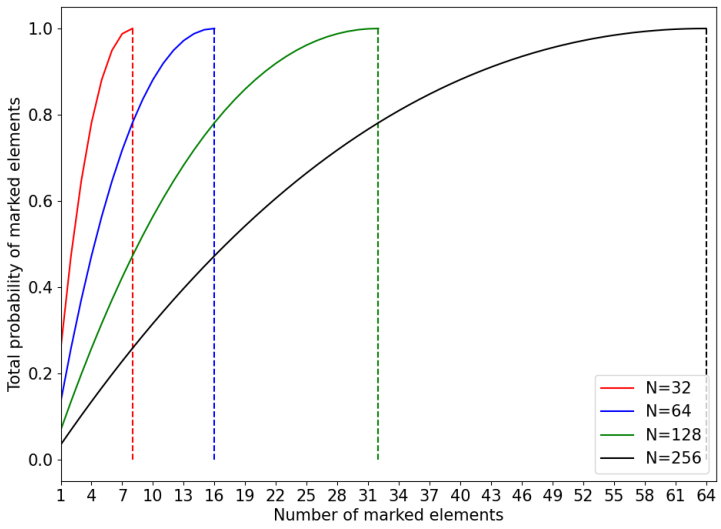

Figure 15: Single Shot temp

reflects the only relevant one in this context. As a consequence, amplitudes associated with state $|\Psi(k_1, l_1)\rangle$ become

$$\begin{cases} k_1 = \frac{1}{\sqrt{t}} \sin\left((2+1)\theta\right) = \frac{1}{\sqrt{\frac{N}{4}}} \sin\left(3\frac{\pi}{6}\right) = \frac{2}{\sqrt{N}} \\ l_1 = \frac{1}{\sqrt{N-t}} \cos\left((2+1)\theta\right) = \frac{1}{\sqrt{N-\frac{N}{4}}} \cos\left(3\frac{\pi}{6}\right) = 0. \end{cases} \tag{60}$$

These results show that the amplitudes associated with the marked states double in relation to $|\Psi_0\rangle$ and the remaining states disappear after only one iteration. This behaviour can be seen in figure 15, where the total probability of marked elements reaches 1 once the number of marked elements is $\frac{1}{4}$ of the total elements.

3.2 COINED QUANTUM WALK

In classical computation, a *spatial search problem* focuses on finding marked points in a finite region of space. Defining this region with graphs is fairly straightforward, the vertices of the graph are the search space, and the edges define what transitions are possible through the search space. As was previously mentioned in **??**, exhaustively searching through an unstructured space, by means of a classical random walk for example, would mean that in the worst case, one would have to take as many steps to find the marked points as there are vertices in the graph. Quantum computing provides an alternative to this complexity through Grover's algorithm, and applying some of his ideas to the coined quantum walk not only allows a quantum counterpart to the random walk search, but also further insight into the algorithm itself.

Following Portugal (2018)'s definition, a good first step is to borrow the diffusion from Grover's algorithm and invert the sign of the state corresponding to the marked vertex while leaving unmarked vertices unchanged. This is done through the following operator

$$\mathcal{O} = I - 2 \sum_{x \in M} |x\rangle \langle x| \tag{61}$$

where M is the set of marked vertices and $\mathcal{O}$ is an analogue to Grover's oracle. For one marked vertex, this oracle can be written as

$$\mathcal{O} = I - 2 |0\rangle \langle 0| \tag{62}$$

Notice that there is no loss of generality by choosing the marked vertex as 0, since the labelling of the vertices is arbitrary.

The next step is to combine the evolution operator from the coined quantum walk model with the oracle

$$U' = U\mathcal{O} \tag{63}$$

Similarly to the simple coined case, the walker starts at $|\Psi(0)\rangle$ and evolves following the rules of an unitary operator U followed by the sign inversion of marked vertices. The walker's state after an arbitrary number of steps will be

$$\Psi(t) = (U')^t \, |\Psi(0)\rangle \, . \tag{64}$$

For a better understanding of the search problem in the coined quantum walk model, consider a graph where all the vertices are connected and each vertex has a loop that allows transitions to itself, as shown in figure **??**. The next step is to label the arcs using notation $\{(v, v'), v \geqslant 0 \wedge v' \leqslant N-1\}$ where N is the total number of vertices and (v, v') are the position and coin value, respectively, in the coined model. The shift operator, now called *flip-flop* shift operator, is

$$S \, |v1\rangle \, |v2\rangle = |v2\rangle \, |v1\rangle \, . \tag{65}$$

The coin operator is defined as

$$C = I_N \otimes G \tag{66}$$

where

$$G = 2 \, |D\rangle \, \langle D| - I \tag{67}$$

is the Grover coin with $|D\rangle$ being the diagonal state of the coin space. Given both of these operators, the evolution is defined for the unmarked case similarly to **??**

$$U = S(I \otimes G). \tag{68}$$

Marking an element in a complete graph is done through the following oracle

$$\mathcal{O}' = \mathcal{O} \otimes I = (I_N - 2 \, |0\rangle \, \langle 0|) \otimes I_N = I_{N^2} - 2 \sum_v |0\rangle \, |v\rangle \, \langle 0| \, \langle v| \, , \tag{69}$$

that can be seen, in the arc notation, as an operator that marks all arcs leaving 0.

Recalling 63, the modified evolution operator can be written as

$$U' = S(I \otimes G)\mathcal{O}' = S(I \otimes G)\mathcal{O} \otimes I = S(\mathcal{O} \otimes G), \tag{70}$$

and the state of the system will evolve according to equation 64.

As was shown in Portugal (2018), maximum probability of the marked vertex is achieved after $\frac{\pi}{2}\sqrt{N}$ steps. Figure 16 is the result of coding and plotting the evolution of this probability distribution, for graphs of varying sizes. It shows that the probability is close

to one at *approximately* the predicted ideal steps, because of the discrete nature of the walk. The probability distributions have a stair-like shape, because transitions in this model only occur on even numbered time steps, because of how the unmodified evolution operator was constructed.

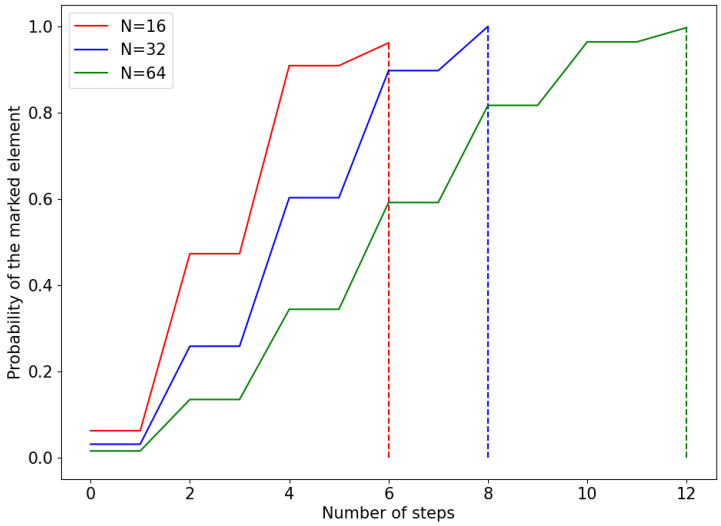

Figure 16: Discrete-time coined quantum walk search for a complete graph with 16, 32 and 64 nodes.

3.3 STAGGERED QUANTUM WALK

The process for defining the search problem in this model is similar to the coined quantum walk case. The oracle still inverts the sign of a certain state and amplifies it, and the system's state will still be described by equation 64. However,instead of using a coin, the staggered model takes advantage of the notions of cliques and tessellations, as was shown in chapter **??**, which means the unmodified evolution operator has to be defined for an undirected complete graph.

As was shown in figure **??**, the vertices in a complete graph are all neighbors. This is a special case because this is the only connected graph where the tessellation cover can be done by one tessellation, since the graph is it's own clique. The minimum tessellations required to cover this structures are defined by the one clique that encompasses all N nodes of the graph

$$\mathscr{T}_\alpha = \{\{0,1,2,...,N-1\}\}. \tag{71}$$

The associated polygon can then be described as the balanced superposition of all the nodes in the graph

$$|\alpha\rangle = \frac{1}{\sqrt{N}} \sum_{v=0}^{N-1} |v\rangle \,. \tag{72}$$

The Hamiltonian, as defined in 18, is

$$H_\alpha = 2 \sum_{0}^{1} |\alpha\rangle \langle\alpha| - I = 2 |\alpha_0\rangle \langle\alpha_0| - I \tag{73}$$

The unmodified evolution operator from equation 19

$$U = e^{i\theta_k H_k} ... e^{i\theta_2 H_2} e^{i\theta_1 H_1} \tag{74}$$

reduces to the single Hamiltonian case

$$U = e^{i\theta H_\alpha}. \tag{75}$$

The choice of the θ value is an important one, since maximum probability is achieved at $\theta = \frac{\pi}{2}$, as shown in figure 17. Since $H_\alpha^2 = I$, equation 75 can be rewritten as

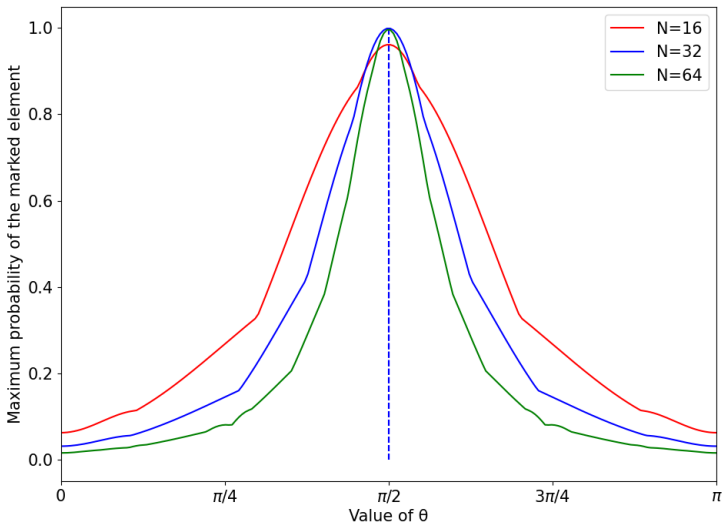

Figure 17: Maximum probability of the marked element as a function of the θ value plotted from 0 to π for number of nodes $N = 64, 128$ and 256.

$$U = e^{-i\frac{\pi}{2}H_\alpha} = \cos\frac{\pi}{2} I + i \sin\frac{\pi}{2} H_\alpha = iH_\alpha = i(2 |\alpha_0\rangle \langle\alpha_0| - I). \tag{76}$$

Having defined the the evolution operator associated with the complete graph, the next step is to use the oracle

$$\mathcal{O} = I_N - 2\left|0\right\rangle\left\langle 0\right|, \tag{77}$$

to create the modified evolution operator associated with the search

$$U' = U\mathcal{O}. \tag{78}$$

The walk achieves the same result as Grover's algorithm after $\frac{\pi}{4}\sqrt{N}$ steps, as shown in figure 18. This plot also shows that the probabilities converge to 1 as N increases, this is because time is discretized and deviations to the ideal steps will matter less for bigger values of N.

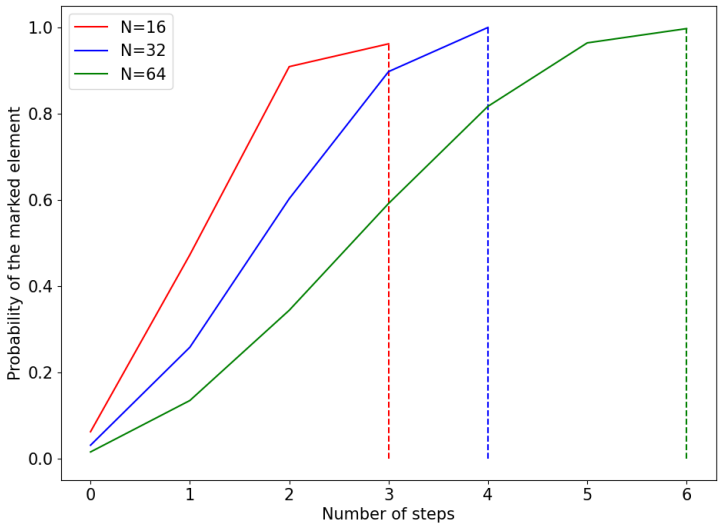

Figure 18: Staggered quantum walk search for a complete graph with 16, 32 and 64 nodes.

3.4 CONTINUOUS-TIME QUANTUM WALK

As was previously seen, the continuous-time quantum walk model is defined by an evolution operator obtained by solving Schrödinger's equation

$$U(t) = e^{-iHt}. \tag{79}$$

The search problem requires introducing an oracle to the Hamiltonian, that will mark an arbitrary vertex m

$$H' = -\gamma L - \left|m\right\rangle\left\langle m\right|. \tag{80}$$

Since the complete graph is a regular graph, the operator can be rewritten in terms of the adjacency matrix plus the marked element. Considering $|0\rangle$ is marked,

$$U'(t) = e^{iH't} = e^{i(-\gamma L - |0\rangle\langle 0|)t} = e^{i(-\gamma A + \gamma D - |0\rangle\langle 0|)t} = e^{-i\gamma(A+|0\rangle\langle 0|)t + i\gamma Dt}. \tag{81}$$

The degree matrix is again $D = dI$, which means it will commute with $A + |0\rangle\langle 0|$ and become a global phase

$$U'(t) = e^{-i\gamma(A+|0\rangle\langle 0|)t} e^{i\gamma Dt} = \phi(t) e^{-i\gamma(A+|0\rangle\langle 0|)t}. \tag{82}$$

As was show by Zalka (1999), the value of γ is crucial for the success of the search. As γ increases, the contribution of the marked element in the Hamiltonian decreases, and as γ approaches 0 the contribution of the adjacency matrix decreases. To find the optimum value, the Hamiltonian can be rewritten by adding multiples of the identity matrix to the adjacency matrix

$$H' = -\gamma(A + NI) - |0\rangle\langle 0| = -\gamma N |s\rangle\langle s| - |0\rangle\langle 0| \tag{83}$$

where $|s\rangle = \frac{1}{\sqrt{N}} \sum_i |i\rangle$. Now it is obvious that, for $\gamma = \frac{1}{N}$, the Hamiltonian is $H = -|s\rangle\langle s| - |0\rangle\langle 0|$. It's eigenstates are proportional to $|s\rangle \pm |w\rangle$ and eigenvalues are $-1 - \frac{1}{\sqrt{N}}$ and $-1 + \frac{1}{\sqrt{N}}$, respectively. This means that the evolution rotates from the state of balanced superposition to the marked vertex state in time $\frac{\pi}{\Delta E} = \frac{\pi}{2}\sqrt{N}$ which is, as was shown by Zalka (1999), optimal and equivalent to Grover's algorithm. Plotting ΔE as a function of γN, as can be seen in figure 19, has a minimum at $\gamma N = 1$. The difference between the largest eigenvalue and second largest, plotted in the y-axis, is the smallest for a value of $\gamma N = 1 \implies \gamma = \frac{1}{N}$, which will correspond to the maximum probability for the marked vertex, in optimal steps.

Figure 20 shows the evolution of the probability of the marked vertex in time, which is continuous in this model. In contrast with previous models, the distributions are smooth and reach exactly one, since the walk is allowed to evolve to exactly the ideal time steps.

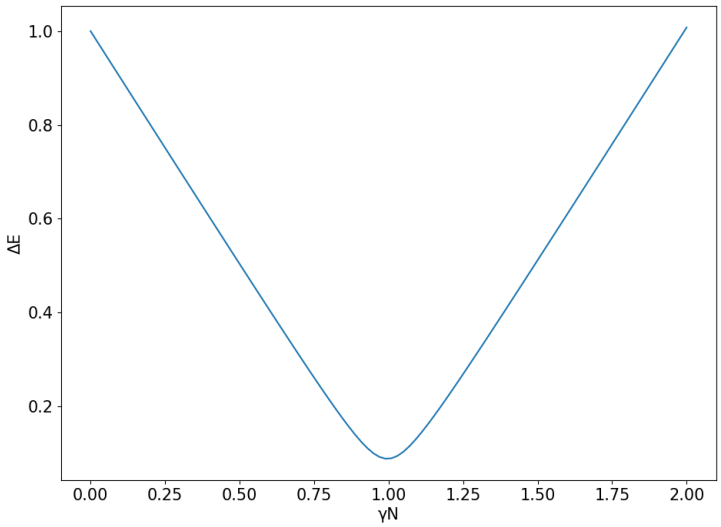

Figure 19: Value of the difference between the largest eigenvalue and the second largest, plotted as a function of γN, for $N = 512$.

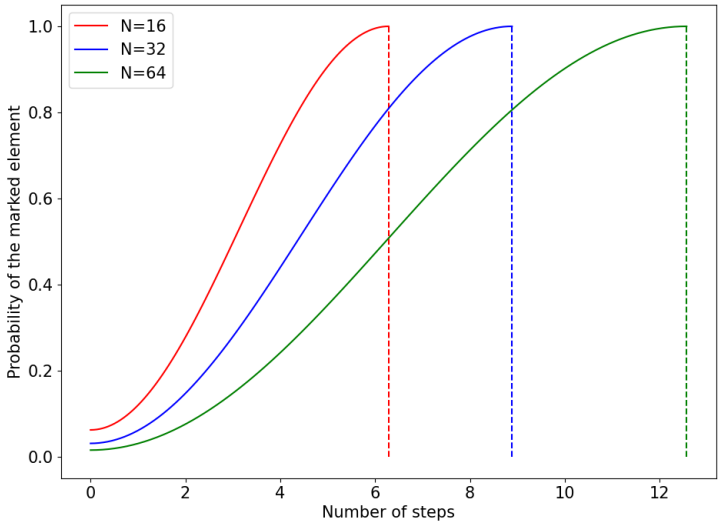

Figure 20: Continuous quantum walk search for a complete graph with 16, 32 and 64 vertices.

4

IMPLEMENTATIONS AND APPLICATIONS

4.1 COINED

Consider the example of a quantum walker on a discretely numbered cycle. It was seen that the evolution operator associated with such a system is, as was defined in equation 6

$$U = S(C \otimes I), \tag{84}$$

where S is a shift operator, defined in equation 5 as

$$S = |0\rangle\langle 0| \otimes \sum_{x=-\infty}^{x=\infty} |x+1\rangle\langle x| + |1\rangle\langle 1| \otimes \sum_{x=-\infty}^{x=\infty} |x-1\rangle\langle x|, \tag{85}$$

that increments or decrements the position of the walker according to the coin operator C.

Previously, this system was simulated in Python by implenting it's equations. Now, the focus is to study a quantum circuit based on the work presented by Douglas and Wang (2009). This approach relies on multi-controlled CNOT gates in order to shift the state of the walker by $+1$ or -1, each with a probability associated with the chosen coin, as can be seen in figure 21.

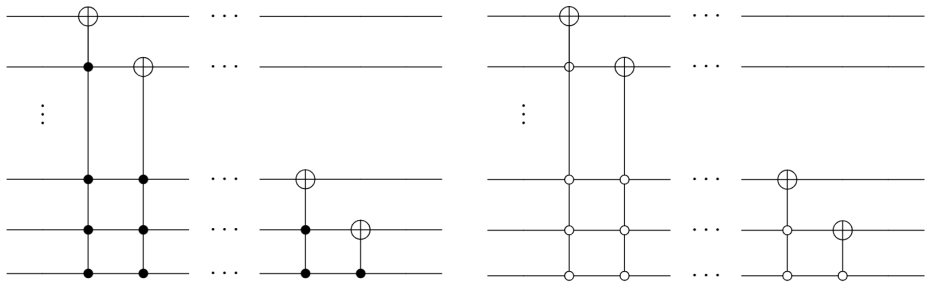

(a) Increment (b) Decrement

Figure 21: Shift operators.

The generalized CNOT gates act on the node states as a cyclic permutator, where each node is mapped to an adjacent state. This can be seen as the walker moving left or right, in the uni-dimensional graph example.

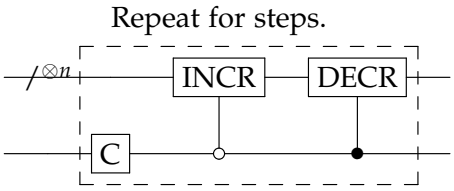

Figure 22: Coined quantum walk circuit

The coin operator will simply be a Hadamard gate acting on a single qubit. For a graph with 16 nodes, for example, 4 qubits are required to encode each node and an extra qubit for the coin. The circuit will then be as shown in figure 22. Note that this circuit limits the number of graph nodes to powers of 2, and an arbitrary implementation of 2^n nodes requires $n+1$ qubits. However, it is possible to have any number of nodes, given that the proper correction is made as can be seen in Douglas and Wang (2009). The method used was *Gray Code Ordering* proposed by Slepoy (2006), whereby a certain arrangement of CNOT gates results in control states only differing by a single bit.

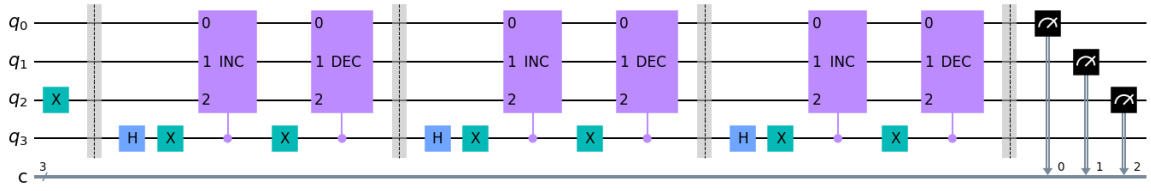

Figure 23: Temp

This circuit was implemented in Qiskit, as can be seen in figure 23. In this example, the increment and decrement sequence was applied three times on a graph of size $2^3 = 8$ nodes. The starting position of the walker was set to $\Psi(0) = |4\rangle$, and the Hadamard coin was used. The first block after the barrier is the sequence of operations that will increment the state of the walker, as is shown in figure 24. The generalized NOT gates are implemented using Qiskit's *mcx* function, which implements the decomposition present in lemma 7.5 of Barenco et al. (1995) to create CNOT gates up to four controls, and the aforementioned Gray Code for more generalized instances of the gate. The next set of operations perform the decrement of the state of the walker, which is just an increment block with it's controls negated as is shown in figure 25. The rest of the circuit is just the repetition of these operations as a function of the number of steps required.

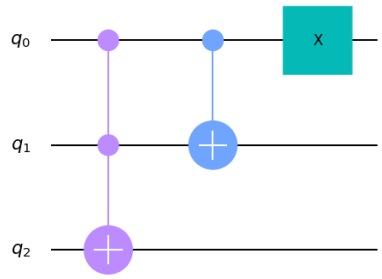

Figure 24: Temp

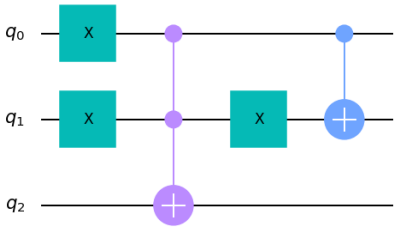

Figure 25: Temp

Lastly, the circuit is measured and the results can be seen in figure 26. These results can be verified by calculating the time evolution of the wave function associated with the system

$$|\Psi(0)\rangle = |4\rangle \tag{86}$$

$$|\Psi(1)\rangle = \frac{|0\rangle\,|x=3\rangle + |1\rangle\,|x=5\rangle}{\sqrt{2}} \tag{87}$$

$$|\Psi(2)\rangle = \frac{|0\rangle\,|x=2\rangle + |1\rangle\,|x=4\rangle + |0\rangle\,|x=4\rangle - |1\rangle\,|x=6\rangle}{2} \tag{88}$$

$$|\Psi(3)\rangle = \frac{|1\rangle\,|x=1\rangle - |0\rangle\,|x=3\rangle + 2(|0\rangle + |1\rangle)\,|x=5\rangle + |0\rangle\,|x=7\rangle}{2\sqrt{2}}. \tag{89}$$

Taking the modulus squared of the amplitudes associated with the states, confirms that the probability distribution associated with the *Qasm* simulator, presented in figure 26 as the blue bar plot, is correct. However, the results obtained from running in IBM's *Toronto* backend are not satisfactory. This is because of the size of the circuit, the coined quantum walk model besides requiring an extra qubit for the coin, also needs a very large number of CNOT gates, which have an average associated error of $1.284e-2$ in this specific backend.

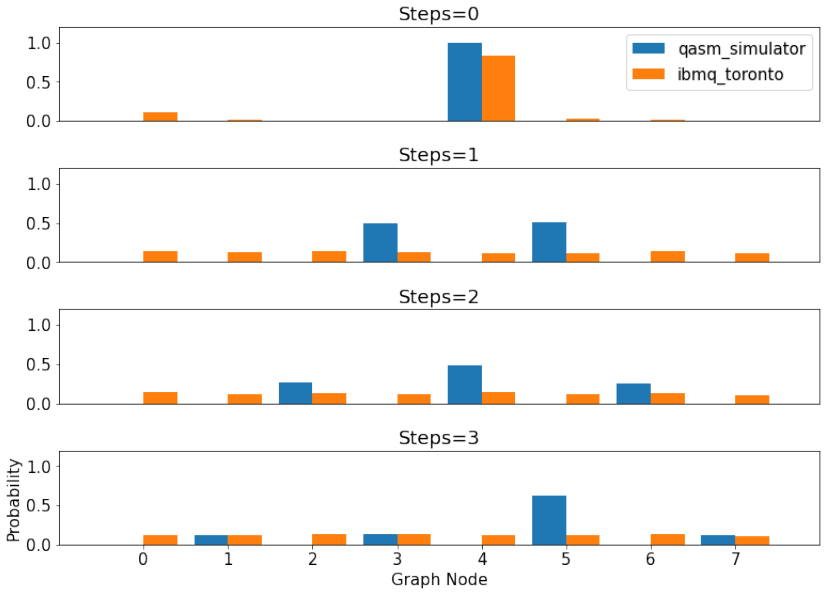

Figure 26: Temp

For a better analysis of the error, one can calculate the fidelity between the ideal distribution $p(x)$ and the experimental $q(x)$ using the formula

$$F(p,q) = \sum_{x=0}^{N-1} \sqrt{p(x)q(x)} \tag{90}$$

where x is the vertex. For 0 steps, the obtained fidelity is approximately 0.91 which is very high, because the circuit is simply the initial condition, and when the circuit is increased to 1 step the fidelity lowers to 0.49, due to the increase of CNOTS. However, for 2 and 3 steps, the fidelity increases again to approximately 0.63 due to the fact that the probability distribution in the simulator becomes more spread out with the increase of steps, meaning that the random uniform distribution obtained from the noisy experiments ran in IBM's backend will be closer to them than a highly localized distribution like in the case of 1 step.

In order to curb the effects introduced by noise, the next chapter will present the circuit for the alternative discrete model, the staggered quantum walk. Besides not needing an extra qubit for the coin, this model also does not require as many CNOT gates for each iteration.

4.2 STAGGERED

As was seen in section 2.3, the elements of each tesselation of a discretely numbered cycle can be described by states

$$|\alpha_x\rangle = \frac{|2x\rangle + |2x+1\rangle}{\sqrt{2}} \tag{91}$$

$$|\beta_x\rangle = \frac{|2x+1\rangle + |2x+2\rangle}{\sqrt{2}}. \tag{92}$$

These states allow the construction of the Hamiltonians

$$H_\alpha = 2\sum_{x=-\infty}^{+\infty} |\alpha_x\rangle \langle\alpha_x| - I \tag{93}$$

$$H_\beta = 2\sum_{x=-\infty}^{+\infty} |\beta_x\rangle \langle\beta_x| - I \tag{94}$$

as was seen in equations 25 and 26. As was shown by Acasiete et al. (2020), these operators cane be rewritten in matrix form

$$H_\alpha = I \otimes X \tag{95}$$

$$H_\beta = \begin{pmatrix} 0 & \cdots & 1 \\ \vdots & H_\alpha & \vdots \\ 1 & \cdots & 0 \end{pmatrix} \tag{96}$$

which are very useful representations when constructing the circuit.

As was shown in equation **??**, the unitary evolution operator is

$$U = e^{i\theta H_\beta} e^{i\theta H_\alpha} = U_\beta U_\alpha, \tag{97}$$

and knowing that

$$R_x(\theta) = e^{\frac{-i\theta X}{2}}, \tag{98}$$

then each of the operators associated with the different tesselation Hamiltonians can be written as

$$U_\alpha = I \otimes R_x(\theta) \tag{99}$$

$$U_\beta = \begin{pmatrix} \cos\theta & \cdots & -i\sin\theta \\ \vdots & U_\alpha & \vdots \\ -i\sin\theta & \cdots & \cos\theta \end{pmatrix} \tag{100}$$

Notice that U_β is simply a permutation of U_α and can be rewritten as

$$U_\beta = P^{-1} U_\alpha P \tag{101}$$

where $P = \sum_x |x+1\rangle \langle x|$. Remember from equation 85 and figure **??** that these permutation operators can be implemented as increment and decrement gates, defined in the work of

Douglas and Wang (2009). Therefore, the circuit for the staggered quantum walk on the line can be constructed as is shown in figure 27.

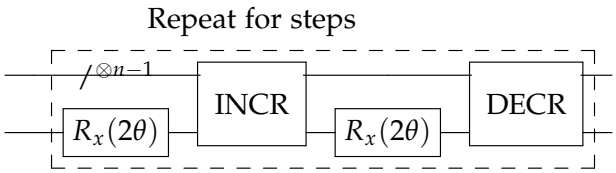

Figure 27: Staggered quantum walk circuit

The next step is to implement the circuit in Qiskit, in order to test it in a real quantum computer. Here, the walk will take place in a cyclic graph with 8 elements, meaning 3 qubits will be required as is shown in figure 28.

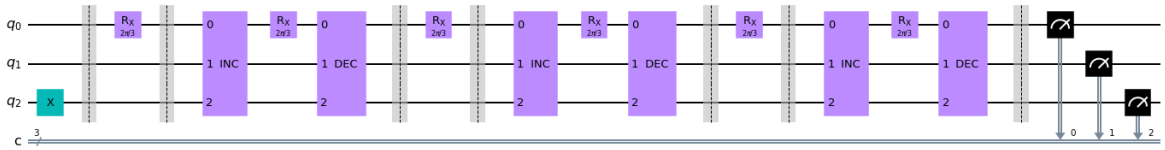

Figure 28: Temp

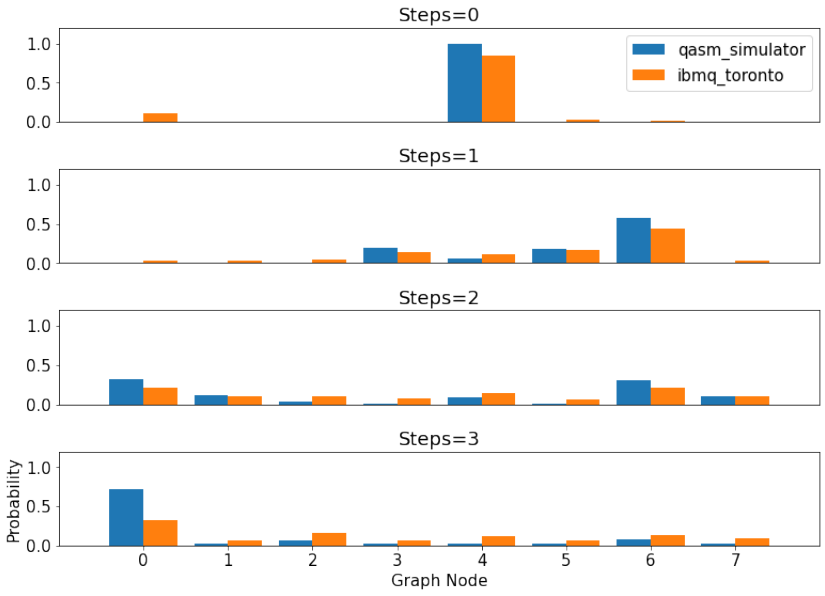

Figure 29: Temp

The circuit starts with a Pauli-X gate in the third qubit so that $|\psi_0\rangle = |4\rangle$. The following operation is a rotation in the X basis, where $\theta = \frac{\pi}{3}$ since it was seen in figure 5 that this value of θ maximizes the propagation of the walk. Finally, U_β is applied, making use of

the increment and decrement gates defined in figures 24 and 25. Note that now, because this model is does not require a coin, these gates do not need to be controlled, meaning that one less qubit is needed for the walk and one less multi-controlled NOT gate will be implemented, making it more NISQ computer friendly. This procedure is repeated 3 times, and the resulting probability distributions after measurement can be seen in figure 29.

Analyzing the figure, it is clear that this model is much better suited for running in a NISQ computer. Even though the probability distribution was somewhat affected by noise, the dynamics of the walk can be seen in the Toronto backend experiment. Highest fidelity was achieved for 2 steps, with a value of approximately 0.95, and the remaining steps ranging from 0.91 to 0.92. Again, it may seem counter-intuitive that a higher fidelity is achieved for a larger circuit, compared to 0 steps for example, but this is again due to the balance of circuit size and spread of the probability distribution. Nevertheless, because this discrete model requires ever more operations with the increase of steps, it will eventually become intractable for NISQ technology. For this reason, the next model studied in this work is one where the circuit will be constant in time.

4.3 CONTINUOUS

As was seen in section 2.4, the unitary evolution operator of this model is defined as

$$U(t) = e^{-iHt} = e^{i(-\gamma L)t} = e^{-i\gamma(A+D)t}. \tag{102}$$

Considering a regular graph, this operator can be rewritten as

$$U(t) = \phi(t)e^{-i\gamma(A)t}, \tag{103}$$

where $\phi(t)$ is a global phase and A is the adjacency matrix associated with the graph.

Here, the study will focus on the circuit implementation of this walk in a cyclic graph, and a different approach was used to define the adjacency matrix. This approach relies on the concept of a circulant graph, which are a class of graphs defined by a circulant matrix such that

$$A = \begin{pmatrix} c_0 & c_{N-1} & \cdots & c_3 & c_2 \\ c_1 & c_0 & c_{N-1} & & c_3 \\ \vdots & c_1 & c_0 & \ddots & \vdots \\ c_{N-2} & & \ddots & \ddots & c_{N-1} \\ c_{N-1} & c_{N-2} & \cdots & c_1 & c_0 \end{pmatrix}. \tag{104}$$

In order to generate the proper circulant graphs, restrictions on this matrix are needed. Firstly, $c_0 = 0$, since self-loops are not part of the structure. Secondly, the matrix must be symmetric, therefore $c_{n-j} = c_j$.

These matrices can be fully described by the first column of the matrix

$$v_1 = [c_0, c_1, \cdots, c_{N-2}, c_{N-1}]^T \tag{105}$$

with a discrete convolution operator performing cyclic permutations of c, on each column. For example,

$$Dv_1 = [c_{N-1}, c_0, \cdots, c_{N-3}, c_{N-2}]^T = v_2. \tag{106}$$

More specifically, for the cycle case

$$Dv_1 = D[0, 1, 0, \cdots, 0, 1]^T = [1, 0, 1, 0, \cdots, 0, 0]^T = v_2. \tag{107}$$

The eigenvalues of a circulant matrix can be found by

$$\lambda_p = c_0 + \sum_{q=1} c_{N-q} \omega^{pq}, \tag{108}$$

and the eigenvectors are

$$\left|\varphi_p\right\rangle = \frac{1}{\sqrt{n}} \sum_{q=0}^{n-1} \omega^{pq}. \tag{109}$$

This given, it is possible to construct an operator that diagonalizes the circulant matrix through the eigenvectors, which is useful for constructing the circuit. For this purpose, the Quantum Fourier Transform can be used and it is defined as

$$F = \frac{1}{\sqrt{N}} \sum_{p,q} \omega^{pq} \left|p\right\rangle \left\langle q\right|. \tag{110}$$

The adjacency matrix of a circulant graph can then be diagonalized such that

$$A = F^\dagger \Lambda F, \tag{111}$$

where Λ is a diagonal operator that encodes the eigenvalues

$$\Lambda = \sum_j \lambda_j \left|j\right\rangle \left\langle j\right|. \tag{112}$$

The unitary operator of the walk can then be rewritten as

$$U = F^\dagger e^{i\gamma\Lambda t} F \tag{113}$$

where

$$e^{i\gamma\Lambda t} = \sum_j e^{i\gamma\lambda_j t} |j\rangle \langle j| . \tag{114}$$

This representation is very easily translatable to a quantum circuit, as can be seen in figure 30.

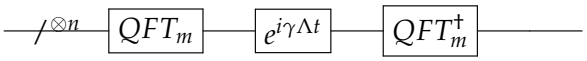

Figure 30: Temp

The circuit can now be constructed making use of the *diagonal* function provided by Qiskit, which decomposes diagonal operators based on the method presented in theorem 7 of Shende et al. (2006). The other tool used was the Quantum Fourier Transform, also provided by the Qiskit package. Figure 31 shows the implementation of the circuit for 3 qubits or $2^3 = 8$ graph nodes and $t = 3$.

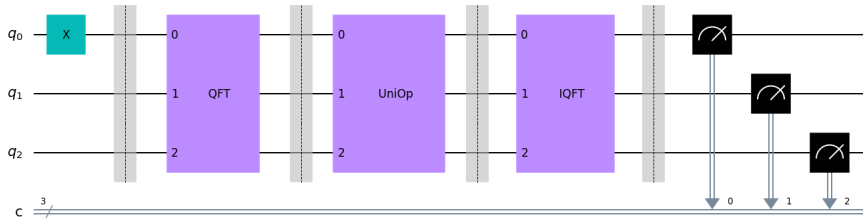

Figure 31: Temp

The circuit for the Quantum Fourier transform is well known and presented in figure 32. The circuit associated with $F^\dagger$ is similarly constructed by negating the previous figure's rotations.

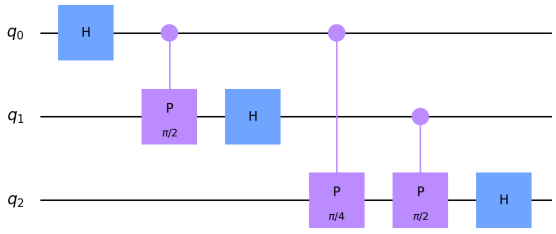

Figure 32: Temp

The circuit associated with the diagonal operator is show in figure 33. Furthermore equation 113 says that time is simply a constant inside the exponential, which means that

the diagonal operator's circuit will not need extra gates when increasing time, it will only need different rotations and differ in global phase. This is an advantage when comparing to

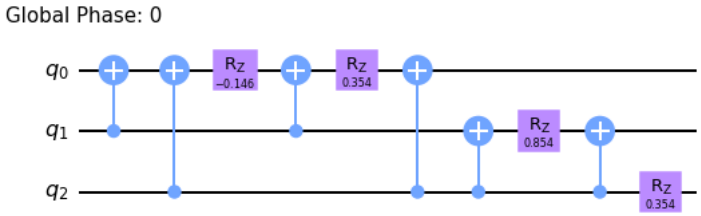

Figure 33: temp

the previous model, seen in figure 23, where each extra step required another increment and decrement gates. Finally, the circuit was measured, and the result can be seen in figure 34. The dynamics of the walk, when ran on the Toronto backend, is closer to the

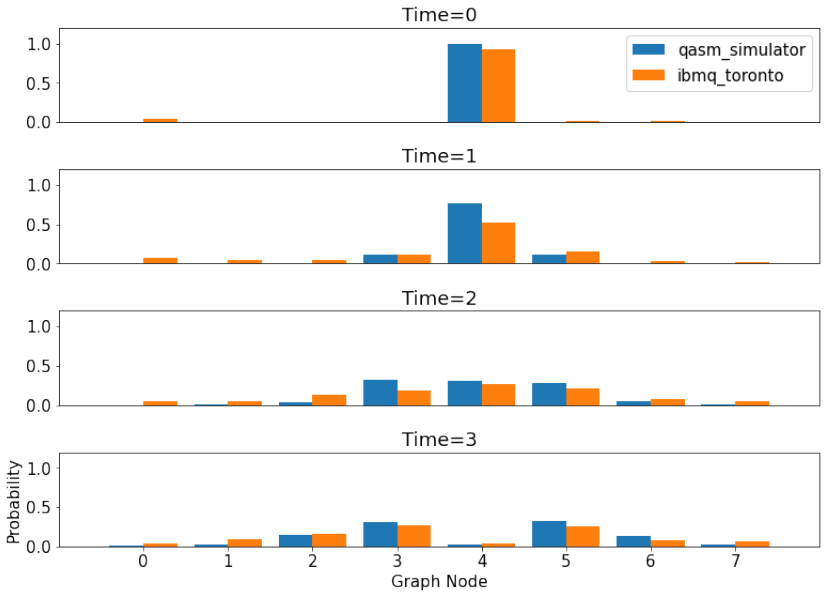

Figure 34: Temp

simulation than the previous examples. As expected, since the size of the circuit does not scale with time, a fidelity of approximately 0.97 was achieved for $t = 3$. For $t = 0, 1, 2$, the respective fidelities were $0.96, 0.90, 0.92$, which are small improvements when compared to the staggered quantum walk, but that stay relatively constant with increasing time, making this type of circuit well suited for studying the dynamics of the continuous-time quantum walk.

Further Experiments

Another improvement can be made to this model by use of the approximate quantum Fourier transform (AQFT). The AQFT, proposed by Coppersmith (2002), is achieved through the modification of the regular quantum Fourier transform circuit, as defined in annex B.1, by removing the phase-shift operations between the most distant qubits. This can be implemented in Qiskit by providing the *QFT* function the approximation degree.

Each experiment is performed 10 times, with 3000 shots each, in order to extract substantial statistical data, using the confidence interval of 95%. The average fidelity between the ideal $p(x,t)$ and the experimental $q(x,t)$ distributions is again calculated using

$$F(p,q) = \frac{1}{10}\sum_{i=1}^{10}\sum_{x=0}^{N-1}\sqrt{p(x,t)q(x,t)}, \tag{115}$$

which is a simple modification of equation 115.

For this section, not only is the cyclic graph considered, but a considerable number of other circulant graph as is shown in figure 35. The numbering of the graphs follows the rule that G_k will have entries $c_k, \cdots, c_1 = 1$ and $c_{n-k}, \cdots, c_{n-1} = 1$, and the remaining elements are 0. This way, it is possible to systematically construct circulant graphs varying from sparse to dense.

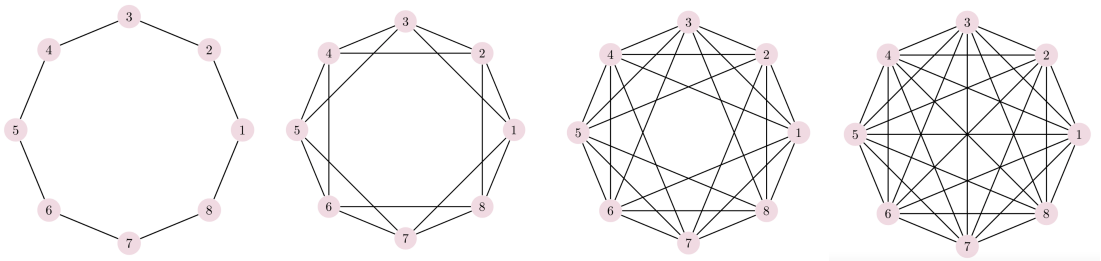

(a) G_1 (b) G_2 (c) G_3 (d) G_4

Figure 35: Circulant graphs G_k for $N = 8$ elements.

Starting with the smaller $N = 2^2 = 4$ case, two non-isomorphic circulant graphs are possible to construct. G_1 corresponds to the cycle graph, and G_2 to the complete graph. Table 1 shows the achieved average fidelities, which were calculated with equation 115. Comparing to the complete graph case presented in Qiang et al. (2016), where they obtained a fidelity of 0.967 ± 0.003, it is possible to see that the implementation presented here slightly outperforms it in terms of fidelity.

In the $N = 2^3 = 8$ case, table 2 shows that state fidelity is greater as graph connectivity increases, and as m increases. This is due to the fact that a greater m implies a smaller circuit, but also an increase in error. However, graphs have less distinct eigenvalues as they are more connected, which means that a higher degree of approximation of the QFT will generally

m\G	G_1	G_2
0	0.98 ± 0.01	0.99 ± 0.01
1	0.98 ± 0.02	0.993 ± 0.006

Table 1: Fidelity of quantum state with N=4, backend *Toronto*, and t=1.

introduce less error in this cases, while keeping circuit depth lower. Finally, table 3 presents

m\G	G_1	G_2	G_3	G_4
0	0.80 ± 0.01	0.92 ± 0.02	0.968 ± 0.007	0.965 ± 0.006
1	0.894 ± 0.007	0.95 ± 0.01	0.98 ± 0.01	0.973 ± 0.008
2	0.852 ± 0.009	0.955 ± 0.004	0.985 ± 0.003	0.990 ± 0.002

Table 2: Fidelity of quantum state with N=8, backend *Toronto*, and t=1.

m\G	G1	G2	G3	G4	G5	G6	G7	G8
0	0.47 ± 0.03	0.61 ± 0.02	0.78 ± 0.02	0.86 ± 0.01	0.86 ± 0.01	0.70 ± 0.04	0.54 ± 0.03	0.49 ± 0.04
1	0.50 ± 0.03	0.63 ± 0.03	0.79 ± 0.03	0.87 ± 0.02	0.85 ± 0.03	0.70 ± 0.03	0.55 ± 0.05	0.50 ± 0.04
2	0.55 ± 0.03	0.71 ± 0.03	0.83 ± 0.02	0.90 ± 0.01	0.89 ± 0.02	0.75 ± 0.02	0.62 ± 0.04	0.59 ± 0.06
3	0.60 ± 0.03	0.70 ± 0.02	0.85 ± 0.01	0.92 ± 0.01	0.91 ± 0.01	0.80 ± 0.03	0.71 ± 0.04	0.69 ± 0.04

Table 3: Fidelity of quantum state with N=16, backend *Toronto*, and t=1.

the $N = 2^4 = 16$ case. Here, the behaviour is similar to the previous case up to graph G_5, meaning that higher graph connectivity and larger m will result in higher fidelity. However, graphs G_6, G_7 and G_8, even though are highly connected and have relatively low depth, present lower fidelity. This seems to contradict the results in table 2, however this behavior can be explained due to the fact that the probability distribution of the dynamics of the walk on these structures is highly concentrated in a small number for vertices. Considering that the size of the circuit starts to push the limits of NISQ computers, it is expected that the spreading out of the probability distribution due to the effects of noise results in a lower fidelity. Nonetheless, the increase of m still has a positive impact on the fidelity of these circuits, which means that the reduction in circuit size will indeed produce better results.

4.4 Search Problems with Qiskit

4.4.1 *Grover*

As was seen in section **??**, Grover's algorithm is a quantum alternative to unstructured search problems. Consider the case of finding element x_0 out of an unordered list of size N. Worst case scenario, a classical algorithm would need to check every element of the list, requiring N steps.

The first stage of Grover's algorithm is to create an uniform superposition of all states in the system

$$|\Psi_0\rangle = \frac{1}{\sqrt{N}} \sum_{x=0}^{N-1} |x\rangle \,. \tag{116}$$

Next is the application of the Grover iteration process, which starts with an oracle that adds a negative phase to the solution states

$$\mathcal{O} |x\rangle = (-1)^{f(x)} |x\rangle \,. \tag{117}$$

This operator can be seen as an identity matrix with negative entries corresponding to the solution states, and the operator can be rewritten as

$$\mathcal{O} = I - 2 \sum_{m \in M} |m\rangle \langle m| \,. \tag{118}$$

where I is the identity matrix and M is a set of solutions where $f(m) = 1$, otherwise it's 0. The matrix associated with this operator will be

$$\mathcal{O} = \begin{pmatrix} (-1)^{f(0)} & 0 & \cdots & 0 \\ 0 & (-1)^{f(1)} & \cdots & 0 \\ \vdots & 0 & \ddots & \vdots \\ 0 & 0 & \cdots & (-1)^{f(N-1)} \end{pmatrix} . \tag{119}$$

The second part of the iteration is an amplitude amplification process by means of the diffusion operator

$$\mathcal{D} = (2 |\Psi_0\rangle \langle \Psi_0| - I) = H^{\otimes n} (2 |0\rangle \langle 0| - I) H^{\otimes n}. \tag{120}$$

The unitary operator that describes the Grover iteration process will then be

$$\mathcal{U} = \mathcal{D}\mathcal{O}. \tag{121}$$

As was previously discussed in section **??**, this iteration process will be done several times, depending on the number of elements. Optimal probability of success finding a single solution will be reached after $\lfloor \frac{\pi}{4}\sqrt{N} \rfloor$ steps, and $\lfloor \frac{\pi}{4}\sqrt{\frac{N}{K}} \rfloor$ for K solutions, which is a quadratic gain when compared to the classical case. The circuit can then be constructed as is shown in figure 36.

Consider the 3 qubit case, where $N = 8$ and solution state $|4\rangle$. The optimal number of iterations is approximately 2, and figure 37 is the circuit for 3 iterations implemented in Qiskit.

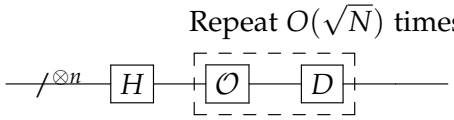

Figure 36: Temp

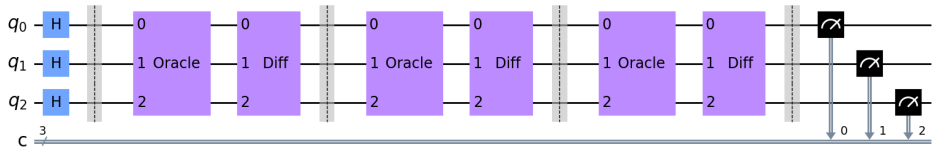

Figure 37: Temp

The system starts with the creation of an uniform superposition state, which means applying Hadamard gates to each qubit. Immediately following the barrier, the first operator

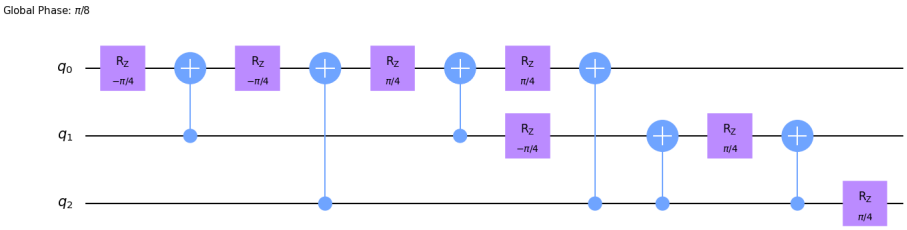

Figure 38: Temp

of the iteration process is the oracle, which is shown in figure 38. Because the oracle operator is simply the identity matrix with negative entries corresponding to the solution states, it can be simply translated into a circuit by means of the diagonal function in Qiskit. The last part of the iteration is the diffusion operator, whose circuit is shown in figure 39. Comparing

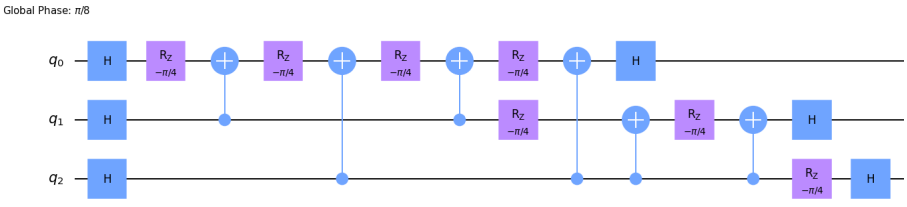

Figure 39: Temp

equations 118 and 120, it is easy to see why figures 38 and 39 are very similar. The diffusion circuit will simply be the oracle circuit for state $|0\rangle$ in between Hadamard operations. The results of measurement are shown in figure 40. As was expected, maximum probability for the marked element was reached after 2 iterations, on the simulator, and it decreases

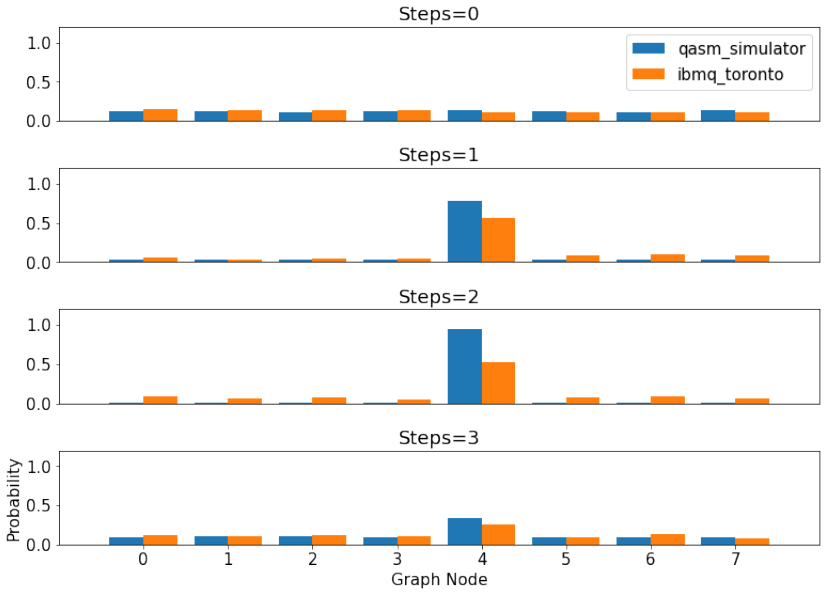

Figure 40: Temp

in subsequent steps. However, the experimental result from the Toronto backend present maximum probability for the marked element for 1 step, with a fidelity of 0.96, and a fidelity of 0.89 for the optimal number of steps steps. This is because as the number of steps increases, so does circuit depth, meaning that the circuit does not achieve the maximum probability after 2 steps due to the effects introduced by noise.

The results, however, are satisfactory when considering the properties of NISQ computers. The following sections will present the search problem adpated to several quantum walk models.

4.4.2 *Coined*

As previously done in section **??**, this chapter aims to expand the coined quantum walk model incorporating concepts like the oracle and diffusion operator of the Grover algorithm. In fact, for the complete graph case, the coined quantum walk and Grover's algorithm are equivalent.

The modified unitary evolution operator is

$$U' = S(\mathcal{O} \otimes G), \tag{122}$$

as was defined in equation 70, where S is the flip-flop shift operator, $\mathcal{O}$ is the oracle operator and G is the Grover diffusion as a coin operator.

Consider the case of a complete graph, where every vertex is adjacent to one another. The quantum circuit to implement this, as shown in figure 41, will require N qubits to represent the state of the walker and N qubits for the state of the coin. The shift operator was constructed based on the work of Douglas and Wang (2009), where the state of the walker is flip-flopped with the state of the coin, which can be done through swap gates.

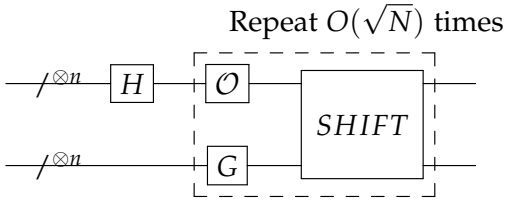

Figure 41: Douglas wang coined quantum walk circuit

This was implemented in Qiskit, for a graph of size $N = 2^3 = 8$, which means 6 qubits will be required. For the case of one marked element, the number of iterations that maximizes the amplitude of the solution state is $\lfloor \frac{\pi}{2}\sqrt{N} \rfloor$, and figure 42 shows the circuit for 5 iterations of the walk.

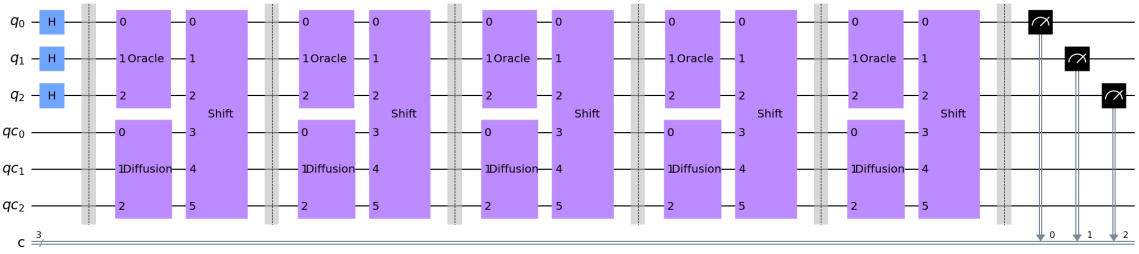

Figure 42: Temp

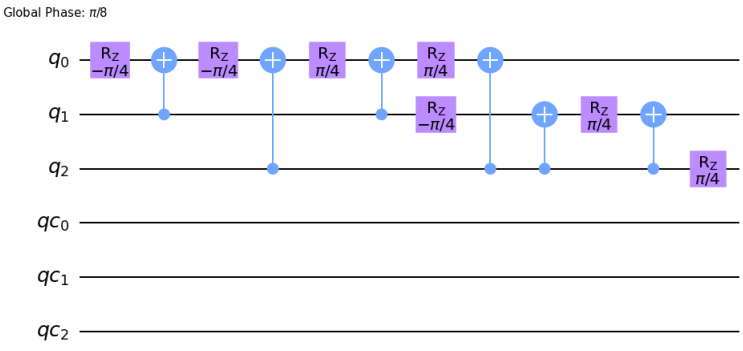

Figure 43: Temp

The circuit starts in a uniform superposition of the states corresponding to the vertices of the graph, and the first step of the iteration is the oracle. This operator will flip the

amplitude of the vertex state $|4\rangle$, and can be translated to a circuit making use of Qiskit's *diagonal*, as is shown in figure 43. It is the same oracle as in the Grover search of figure 38, but in the coined quantum walk model it is only applied to the states associated with the position of the walker. The states associated with the coin space of the walk will be transformed according to Grover's diffusion of figure 39, as is seen in figure 44. The final

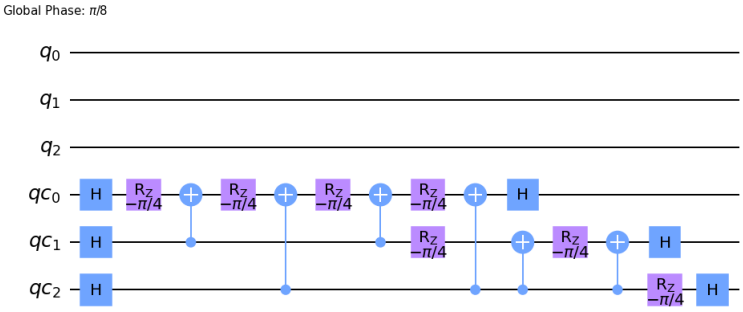

Figure 44: Temp

part of the iteration is the shift operator, as can be seen in figure 45. The flip-flop shift operator was defined in equation 65 as

$$S\,|v1\rangle\,|v2\rangle = |v2\rangle\,|v1\rangle\,, \tag{123}$$

where $|v1\rangle$ represents the position of the walker and $|v2\rangle$ is the state of the coin. Making use of the swap gate, this operator can be implemented as in figure 45.

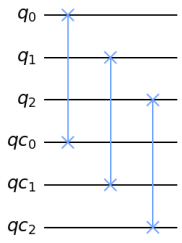

Figure 45: Temp

Lastly, measurements were performed, and the results plotted in figure 46. Maximum probability of the marked element was reached after 4 steps in the simulator, and extra steps reduce said probability. The resulting probability distribution from the Toronto backend is again unsatisfactory for the coined quantum walk model, with fidelities ranging from 0.58 for 4 steps, to 0.75 for 2 steps. This is expected, since the complete graph representation requires N extra qubits for the coin, and swap operations which are decomposed into 3 CNOTs each. The optimal number of steps that maximizes the probability of the marked

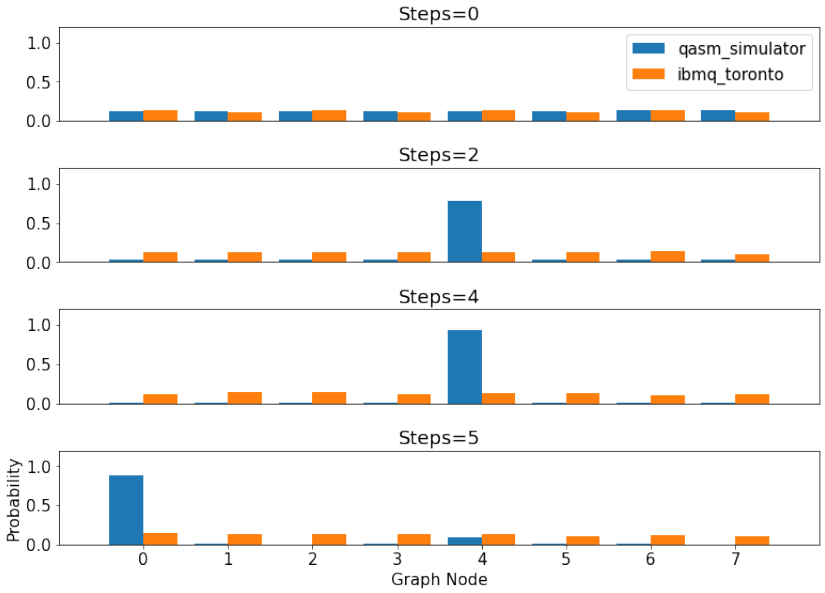

Figure 46: Temp

element is also a contributing factor to the size of the circuit, requiring more iterations to achieve the same probability when compared to Grover's search in the previous chapter.

As was done previously, other models of the quantum walks that do not require coins or iterations will be studied in the following sections, in the context of the searching problem. The staggered quantum walk, for example, should be able to present better results when ran in a NISQ computer, due to its coinless nature.

4.4.3 *Staggered*

Recalling from section 3.3, the staggered quantum walk on a complete graph requires a single tessellation with associated polygon

$$|\alpha\rangle = \frac{1}{\sqrt{N}} \sum_{x=0}^{N-1} |x\rangle \,. \tag{124}$$

The Hamiltonian will then be

$$H_\alpha = 2 \sum_{0}^{1} |\alpha\rangle \langle\alpha| - I = H^{\otimes n}(2 |0\rangle \langle 0| - I) H^{\otimes n} = H^{\otimes n} \mathcal{O}_0 H^{\otimes n}, \tag{125}$$

which is equivalent to the Grover diffusion operator, meaning it can be implemented in a similar fashion. The evolution operator for the staggered quantum walk on the complete graph will then be

$$U = e^{i\theta H_\alpha} = e^{i\theta (H^{\otimes n} \mathcal{O}_0 H^{\otimes n})} = H^{\otimes n} e^{i\theta \mathcal{O}_0} H^{\otimes n}. \tag{126}$$

This is a very useful representation since the exponent part of the operator is a diagonal matrix, which means implementing the circuit in Qiskit is a straightforward task.

Now that the staggered quantum walk associated with the complete graph is defined, what remains is to add an oracle to the evolution operator as was done in equation 78,

$$U' = U\mathcal{O}, \tag{127}$$

where

$$\mathcal{O} = I_N - 2\sum_{m\in M} |m\rangle\langle m|, \tag{128}$$

and M is the set of marked elements.

The general circuit for implementing the staggered quantum walk search problem in a complete graph will then be as shown in figure 47. Since only one tesselation is required,

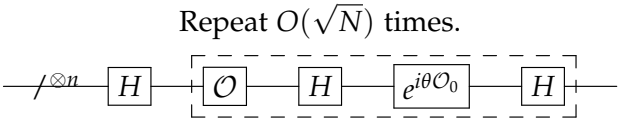

Figure 47: Temp

there is no need for the Suzuki-Trotter aproximation. However, several iterations will be needed in order to achieve maximum probability for the marked vertex. Because the staggered quantum walk search on a complete graph is equivalent to Grover's algorithm, the optimum number of steps will also be $\frac{\pi}{4}\sqrt{\frac{N}{K}}$, where K is the number of solutions.

Consider the case of $N = 8$ and one marked vertex, $|m\rangle = |4\rangle$. The number of steps that maximizes the probability of the marked element is $\frac{\pi}{4}\sqrt{\frac{8}{1}} \approx 2$. Translating to Qiskit, $n = 3$ qubits will be needed and the circuit will be as in figure 48.

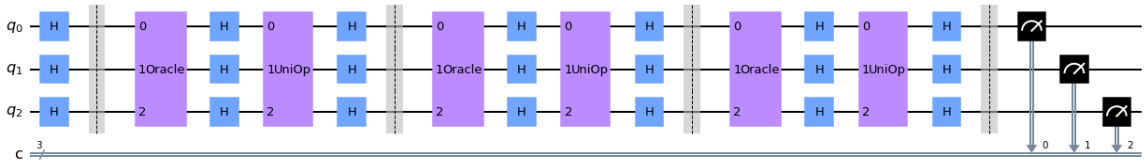

Figure 48: Temp

Similar to previous examples, the circuit begins with the uniform superposition achieved through Hadamard gates. The next operation of the search problem is the oracle, which was implemented through the use of Qiskit's *diagonal* function that produces a circuit similar to the one in figure 38. Next, an analogue of Grover's diffusion operator is applied, where the operation named *UniOp* is a diagonal matrix, easily translated to Qiskit as is shown in figure 49. This circuit is very similar to the one in figure 39, the difference being that

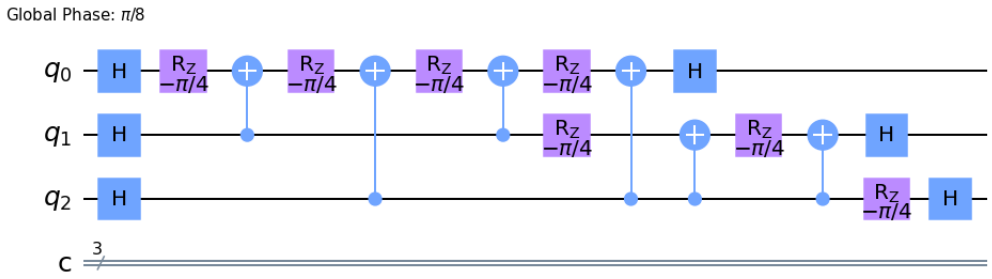

Figure 49: Temp

in the staggered quantum walk search model one can control the value of θ, as can be seen in equation 126, which influences how fast maxmimum probability of the marked element is achieved. Since Grover's algorithm is optimal, a value of $\theta = \frac{\pi}{2}$ yields a diffusion circuit equal to the one in figure 39, implying that the staggered quantum walk is a more general model of quantum searching. Finally, measurement is performed and the resuls for several steps of the walk are shown in figure 50. The circuit for each step of the walk was

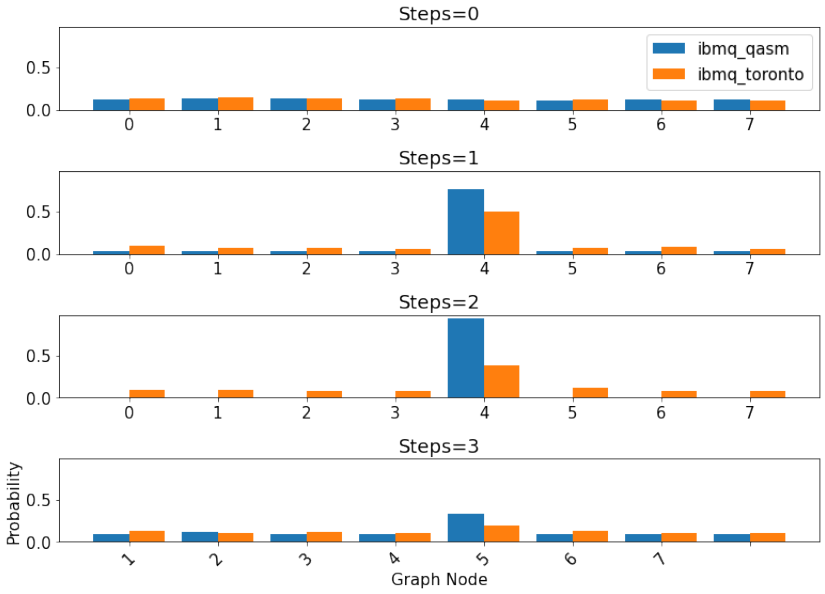

Figure 50: Temp

run both in the *Qasm* simulator and IBM's backend named Toronto. The experiment was performed with 3000 shots in both cases, and the probability distributions show that this model is indeed more suited for a NISQ computer than the previous case. However, unlike the simulator, maximum probability of the marked vertex was achieved withing 1 step of the walk instead of the predicted 2 steps, as was the case of the Grover algorithm. Looking at the 1 step case in the simulator, one can see that the probability of vertex $|4\rangle$ is very close to the maximum, while the circuit has about half of the operations of the 2 step case. This

means it is not surprising that the smaller circuit produces higher results for the probability of the marked vertex. This can be further confirmed by the fidelities of each of the states, which are aproximately 0.954 and 0.780 for 1 step and 2 steps, respectively, implying that the former circuit produces better results because of the number of operations, even though that the latter should theoretically yield the highest probability.

Even though these results are a great improvement to the search problem using the coined quantum walk, the staggered model is still discrete, meaning it's circuit will increase in size as the number of steps increases. This can be avoided by turning again to the continuous-time model, whose circuit will not increase as time increases. However, for the searching problem, the continuous-time model might not have the best results, because it will need iterations due to the Suzuki-Trotter approximation and it will also require extra operations to implement the oracle, which was not the case in the pure dynamics example of section 4.3 .

4.4.4 *Continuous*

As was seen in section **??**, the unitary operator associated with the continuous time quantum walk model can be modified as to mark an element for amplitude amplification

$$U'(t) = e^{iH't} = \phi(t)e^{-i(\gamma A+O)t}, \tag{129}$$

where $\phi(t)$ is a global phase, A is the adjacency matrix and the oracle is defined as

$$O = \sum_{m\in M} |m\rangle \langle m| , \tag{130}$$

where M is the set of marked elements.

This section will focus on constructing and analyzing the circuit form of the continuous-time quantum walk search problem, which will be performed over a complete graph whose adjacency matrix is

$$A = \begin{pmatrix} 0 & 1 & \cdots & 1 & 1 \\ 1 & 0 & \cdots & 1 & 1 \\ & & \vdots & & \\ 1 & 1 & \cdots & 0 & 1 \\ 1 & 1 & \cdots & 1 & 0 \end{pmatrix}. \tag{131}$$

which is simply a matrix with all entries set to 1, except the diagonal. The first step is to borrow the diagonal definition of the adjacency matrix from equation 111

$$A = F^\dagger \Lambda F, \tag{132}$$

and use the Suzuki-Trotter expansion

$$e^{i(H_0+H_1)t} = \lim_{r\to\infty}(e^{i\frac{H_0 t}{r}}e^{i\frac{H_1 t}{r}})^r, \tag{133}$$

to decompose the operator in equation 129

$$e^{i(\gamma A+O)t} = \lim_{r\to\infty}(F^\dagger e^{i\gamma\frac{\Lambda t}{r}}Fe^{i\frac{Ot}{r}})^r, \tag{134}$$

which can be easily translated into circuit form as in figure 51.

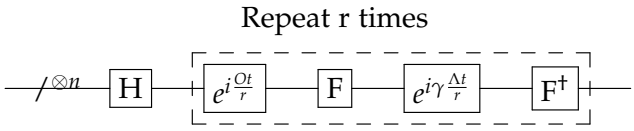

Figure 51: Temp

Consider the case of a graph of size $N = 2^3 = 8$ and trotter number of $r = 1$. The corresponding Qiskit circuit is as shown in figure 51. The system starts out in an uniform

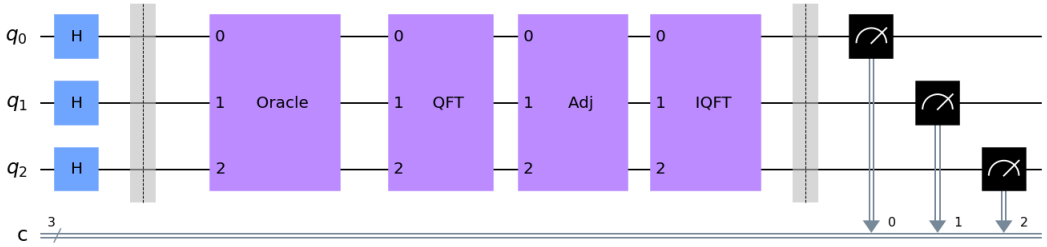

Figure 52: Temp

superposition followed by the application of the oracle operator as can be seen in figure 53. Note that the circuit was obtained by using Qiskit's *diagonal* function that takes the diagonal entries of the operator corresponding to the oracle that was defined in equation 134. The

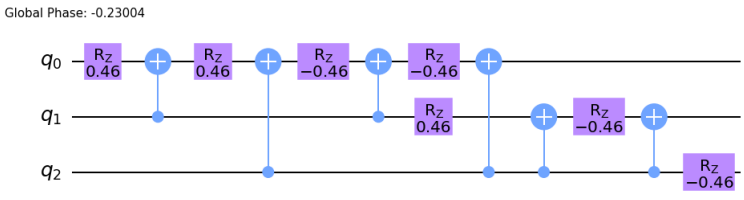

Figure 53: Temp

following operation will be the quantum Fourier transform, but because a complete graph is considered, the AQFT can be used with a degree of $m = 2$, which means the circuit will

simply be Hadamard transforms, thus reducing circuit depth. Lastly, the operator associated with the adjacency matrix is shown in figure 54. Since A is the diagonal adjacency matrix of a complete graph, it is easily implemented using the aforemention *diagonal* function.

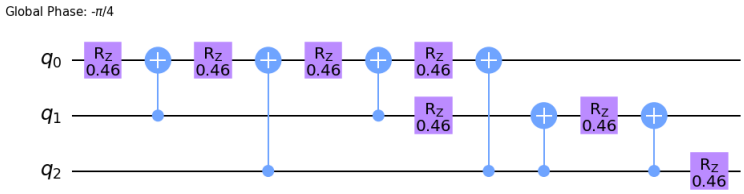

Figure 54: Temp

Finally, the results of circuit measurement can be seen in figure 55. Even though circuit

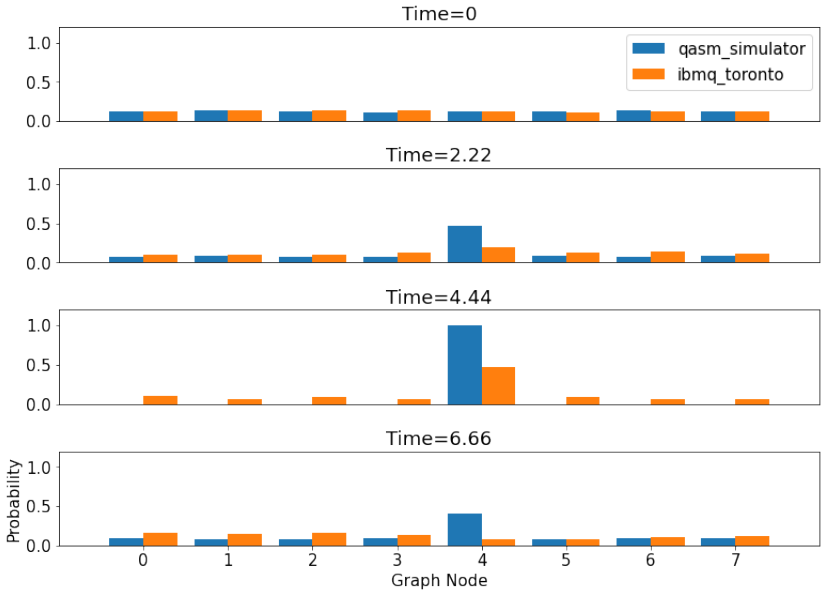

Figure 55: Temp

depth does not scale up with time, introducing the oracle operation to the continuous-time quantum walk model appears to make the circuit hard to run in a NISQ computer. Note that, theoretically, 2 iterations of the Suzuki-Trotter expansion are needed for maximum probability of the marked vertex to be achieved in optimal time. In practice, however, greater probability for this element is achieved when only 1 iteration is performed since the smaller circuit seems to produce a greater fidelity of 0.71, when compared to a fidelity of 0.59 for the 2 iteration case. The approximate quantum Fourier transform also has a positive impact, increasing fidelity from 0.60 when the full QFT circuit is used, to the aforemention 0.71 when only Hadamard transformations are performed.

In conclusion, when comparing the several quantum walk models studied in previous sections, the coined quantum walk seems to be the least suited for running the search problem

in NISQ computers, followed by the continuous-time model which has the advantage of not scaling with time, but produces a circuit slightly too large to achieve fidelities which rival the staggered quantum walk. The latter appears to perform the best because, even though its discrete nature requires several iterations, the circuit depth does not appear to introduce a drastic amount of noise in the $N = 3$ case.

5

DISCUSSIONS AND CONCLUSION

5.1 CONCLUSIONS

Place Conclusions here.

5.2 PROSPECT FOR FUTURE WORK

Place future work here.

BIBLIOGRAPHY

F. Acasiete, F. P. Agostini, J. Khatibi Moqadam, and R. Portugal. Implementation of quantum walks on ibm quantum computers. *Quantum Information Processing*, 19(12), Nov 2020. ISSN 1573-1332. doi: 10.1007/s11128-020-02938-5. URL http://dx.doi.org/10.1007/s11128-020-02938-5.

Dorit Aharonov, Andris Ambainis, Julia Kempe, and Umesh Vazirani. Quantum walks on graphs. *STOC '01 Proceedings of the thirty-third annual ACM symposium on Theory of computing*, pages 50–59, 2001.

Dorit Aharonov, Wim van Dam, Julia Kempe, Zeph Landau, Seth Lloyd, and Oded Regev. Adiabatic quantum computation is equivalent to standard quantum computation. *SIAM Journal on Computing*, 37(1), 2007. doi: 166-194.

Y. Aharonov, L. Davidovich, and N. Zagury. Quantum random walks. *Physical Review A*, 48 (2):1687–1690, 1993.

Andris Ambainis. Quantum walk algorithm for element distinctness. *SIAM Journal on Computing*, 37(1):210–239, 2007.

Radhakrishnan Balu, Daniel Castillo, and George Siopsis. Physical realization of topological quantum walks on ibm-q and beyond. 2017.

Adriano Barenco, Charles H. Bennett, Richard Cleve, David P. DiVincenzo, Norman Margolus, Peter Shor, Tycho Sleator, John A. Smolin, and Harald Weinfurter. Elementary gates for quantum computation. *Physical Review A*, 52(5):3457–3467, Nov 1995. ISSN 1094-1622. doi: 10.1103/physreva.52.3457. URL http://dx.doi.org/10.1103/PhysRevA.52.3457.

Adriano Barenco, Artur Ekert, Kalle-Antti Suominen, and Päivi Törmä. Approximate quantum fourier transform and decoherence. *Physical Review A*, 54(1):139–146, Jul 1996. ISSN 1094-1622. doi: 10.1103/physreva.54.139. URL http://dx.doi.org/10.1103/PhysRevA.54.139.

Paul Benioff. The computer as a physical system: A microscopic quantum mechanical hamiltonian model of computers as represented by turing machines. *Journal of Statistical Physics*, 22(5):563–591, 1980.

Charles Bennett and Gilles Brassard. Withdrawn: Quantum cryptography: Public key distribution and coin tossing. *Theoretical Computer Science - TCS*, 560:175–179, 01 1984. doi: 10.1016/j.tcs.2011.08.039.

Charles H. Bennett and Stephen J. Wiesner. Communication via one- and two-particle operators on einstein-podolsky-rosen states. *Phys. Rev. Lett.*, 69:2881–2884, Nov 1992. doi: 10.1103/PhysRevLett.69.2881. URL https://link.aps.org/doi/10.1103/PhysRevLett.69.2881.

Scott D. Berry, Paul Bourke, and Jingbo B. Wang. qwviz: Visualisation of quantum walks on graphs. *Computer Physics Communications*, 182(10):2295–2302, 2011. ISSN 0010-4655. doi: https://doi.org/10.1016/j.cpc.2011.06.002. URL https://www.sciencedirect.com/science/article/pii/S0010465511002128.

Michael Boyer, Gilles Brassard, Peter Høyer, and Alain Tapp. Tight bounds on quantum searching. *Fortschritte der Physik*, 46(4-5):493–505, 1998.

A. R. Calderbank and Peter W. Shor. Good quantum error-correcting codes exist. *Phys. Rev. A*, 54:1098–1105, Aug 1996. doi: 10.1103/PhysRevA.54.1098. URL https://link.aps.org/doi/10.1103/PhysRevA.54.1098.

D. Cheung. Improved bounds for the approximate qft. 2004.

Chen-Fu Chiang, Daniel Nagaj, and Pawel Wocjan. Efficient circuits for quantum walks. *Quantum Information and Computation*, 10, 03 2009. doi: 10.26421/QIC10.5-6-4.

Andrew M. Childs. Universal computation by quantum walk. *Physical Review Letters*, 102 (18):180501, 2009.

Andrew M. Childs and Jeffrey Goldstone. Spatial search by quantum walk. *Physical Review A*, 70(2):022314, 2004.

Andrew M. Childs, Richard Cleve, Enrico Deott, Edward Farhi, Sam Gutmann, and Daniel A. Spielman. Exponential algorithmic speedup by quantum walk. *Proc. 35th ACM Symposium on Theory of Computing (STOC 2003), pp. 59-68*, 2002. doi: 10.1145/780542.780552.

Paul H. Cootner. *The random character of stock market prices.* M.I.T. Press, Cambridge, Mass, rev. ed. edition, 1967.

D. Coppersmith. An approximate fourier transform useful for quantum factoring. 02 2002.

Gabriel Coutinho and Renato Portugal. Discretization of continuous-time quantum walks via the staggered model with hamiltonians. *Natural Computing*, pages 1–7, 2018.

David Deutsch. Quantum theory, the church-turing principle and the universal quantum computer. *Proceedings of The Royal Society A Mathematical Physical and Engineering Sciences*, 400(1818), 1985.

David Deutsch and Richard Jozsa. Rapid solution of problems by quantum computation. *Proceedings of The Royal Society A Mathematical Physical and Engineering Sciences*, 439(1907), 1992.

B.L. Douglas and J. B. Wang. Efficient quantum circuit implementation of quantum walks. 2009.

Martin Dyer, Alan Frieze, and Ravi Kannan. A random polynomial-time algorithm for approximating the volume of convex bodies. *Journal of the ACM*, 38(1):1–17, 1991.

Matthew D. Falk. Quantum search on the spatial grid. 2013.

Peter E. Falloon, Jeremy Rodriguez, and Jingbo B. Wang. Qswalk: A mathematica package for quantum stochastic walks on arbitrary graphs. *Computer Physics Communications*, 217: 162–170, 2017. ISSN 0010-4655. doi: https://doi.org/10.1016/j.cpc.2017.03.014. URL https://www.sciencedirect.com/science/article/pii/S0010465517301029.

Edward Farhi and Sam Gutmann. An analog analogue of a digital quantum computation. *Physical Review A*, 57(4):2403–2406, 1998.

Edward Farhi, Jeffrey Goldstone, Sam Gutmann, and Michael Sipser. Quantum computation by adiabatic evolution. 2000.

Richard P. Feynman. There's plenty of room at the bottom. *Feynman and computation*, pages 63–76, 1959.

Richard P. Feynman. Simulating physics with computers. *International Journal of Theoretical Physics*, 21(6-7):467–488, 1982.

Steven Finch. "pólya's random walk constant." in mathematical constants. *Cambridge University Press*, pages 322–331, 2003.

Konstantinos Georgopoulos and P. Zuliani. One-dimensional hadamard quantum walk on a cycle with rotational implementation. *arXiv: Quantum Physics*, 2019.

Adam Glos, Jarosław Adam Miszczak, and Mateusz Ostaszewski. Qswalk.jl: Julia package for quantum stochastic walks analysis. *Computer Physics Communications*, 235:414–421, Feb 2018. ISSN 0010-4655. doi: 10.1016/j.cpc.2018.09.001. URL http://dx.doi.org/10.1016/j.cpc.2018.09.001.

Geoffrey Grimmett, Svante Janson, and Petra F. Scudo. Weak limits for quantum random walks. *Physical Review E*, 69(2):026119, 2003.

Lov K. Grover. A fast quantum mechanical algorithm for database search. *STOC '96 Proceedings of the twenty-eighth annual ACM symposium on Theory of computing*, pages 212–219, 1996.

C. A. R. Hoare. Algorithm 64: Quicksort. *Commun. ACM*, 4(7):321, 1961. ISSN 0001-0782. doi: 10.1145/366622.366644. URL https://doi.org/10.1145/366622.366644.

Norio Inui, Yoshinao Konishi, and Norio Konno. Localization of two-dimensional quantum walks. *Physical Review A*, 69(5):052323, 2003.

Josh Izaac and Jb Wang. Pyctqw: A continuous-time quantum walk simulator on distributed memory computers. *Computer Physics Communications*, 186, 01 2015. doi: 10.1016/j.cpc.2014.09.011.

Mark Jerrum, Alistair Sinclair, and Eric Vigoda. A polynomial-time approximation algorithm for permanent of a matrix with nonnegative entries. *Journal of the ACM*, 51(4):671–697, 2004.

Norio Konno. A new type of limit theorems for the one-dimensional quantum random walk. *J. Math. Soc. Japan*, 57(4):1179–1195, 2002.

T Loke and J B Wang. Efficient quantum circuits for continuous-time quantum walks on composite graphs. *Journal of Physics A: Mathematical and Theoretical*, 50(5):055303, Jan 2017a. ISSN 1751-8121. doi: 10.1088/1751-8121/aa53a9. URL http://dx.doi.org/10.1088/1751-8121/aa53a9.

T. Loke and J.B. Wang. Efficient quantum circuits for szegedy quantum walks. *Annals of Physics*, 382:64–84, Jul 2017b. ISSN 0003-4916. doi: 10.1016/j.aop.2017.04.006. URL http://dx.doi.org/10.1016/j.aop.2017.04.006.

Neil B. Lovett, Sally Cooper, Matthew Everett, Matthews Trevers, and Viv Kendon. Universal quantum computation using the discrete quantum walk. *Physical Review A*, 81(4):042330, 2010.

Frédéric Magniez, Ashwin Nayak, Jérémie Roland, and Miklos Santha. Search via quantum walk. *SIAM Journal on Computing*, 40(1):142–164, 2006.

Frédéric Magniez, Miklos Santha, and Mario Szegedy. Quantum algorithms for the triangle problem. *SIAM Journal on Computing*, 37(2):413–424, 2007.

F.L. Marquezino and R. Portugal. The qwalk simulator of quantum walks. *Computer Physics Communications*, 179(5):359–369, Sep 2008. ISSN 0010-4655. doi: 10.1016/j.cpc.2008.02.019. URL http://dx.doi.org/10.1016/j.cpc.2008.02.019.

Elliott Montroll. Random walks in multidimensional spaces, especially on periodic lattices. *Journal of the Society for Industrial and Applied Mathematics*, 4(4):241–260, 1956. doi: 10.1137/0104014.

Elliott Waters Montroll and George Herbert Weiss. Random walks on lattices. ii. *Journal of Mathematical Physics*, page 167–181, 1997.

Gordon E. Moore. Cramming more components onto integrated circuits. *Electronics*, 38(8): 114–117, 1965.

J .K. Moqadam, M. C. de Oliveira, and Renato Portugal. Staggered quantum walks with superconducting microwave resonators. *Physical Review B*, 95(14):144506, 2017.

Rajeev Motwani and Prabhakar Raghavan. *Randomized Algorithms*. Cambridge University Press, 1995.

Ashwin Nayak and Ashvin Vishwanath. Quantum walk on the line. 2000.

Michael A. Nielsen and Isaac L. Chuang. *Quantum Computation and Quantum Information: 10th Anniversary Edition*. Cambridge University Press New York, NY, USA, 2011.

Christos Papadimitrious. *Computational Complexity*. Pearson, 1994.

Apoorva Patel, K.S. Raghunathan, and Pranaw Rungta. Quantum random walks do not need a coin toss. *Physical Review A*, 71(3):032347, 2005.

Karl Pearson. The problem of the random walk. *Nature*, 72(1865):294, 1905. doi: 10.1038/072294b0.

J. Pollard, Lenstra Arjen, H. Lenstra, and Mark Manasse. The number field sieve. 1994.

R. Portugal, R.A.M. Santos, T.D. Fernandes, and D.N. Goncalves. The staggered quantum walk model. *Quantum Information Processing*, 15(1):85–101, 2016.

Renato Portugal. Establishing the equivalence between szegedy's and coined quantum walks using the staggered model. *Quantum Information Processing*, 15(4):1387–1409, 2015.

Renato Portugal. *Quantum Walks and Search Algorithms*. Springer, 2018.

Renato Portugal and T. D. Fernandes. Quantum search on the two-dimensional lattice using the staggered model with hamiltonians. *Physical Review A*, 95(4):042341, 2017.

Renato Portugal, Stefan Boettcher, and Stefan Falkner. One-dimensional coinless quantum walks. *Physical Review A*, 91(5):052319, 2015.

Renato Portugal, M. C. de Oliveira, and J. K. Moqadam. Staggered quantum walks with hamiltonians. *Physical Review A*, 95(1):012328, 2017.

George Pólya. Über eine aufgabe der wahrscheinlichkeitsrechnung betreffend die irrfahrt im straßennetz. *Mathematische Annalen*, 84:149–160, 1921. doi: 10.1007/BF01458701.

Xiaogang Qiang, Thomas Loke, Ashley Montanaro, Kanin Aungskunsiri, Xiaoqi Zhou, Jeremy L. O'Brien, Jingbo B. Wang, and Jonathan C. F. Matthews. Efficient quantum walk on a quantum processor. *Nature Communications*, 7(1), May 2016. ISSN 2041-1723. doi: 10.1038/ncomms11511. URL http://dx.doi.org/10.1038/ncomms11511.

J. J. Sakurai. *Modern Quantum Mechanics*. Addison-Wesley Publishing, Co, 1994.

Miklos Santha. Quantum walk based search algorithms. *International Conference on Theory and Applications of Models of Computation. TAMC 2008. Lecture Notes in Computer Science*, 4978:31–46, 2008.

Marek Sawerwain and Roman Gielerak. Gpgpu based simulations for one and two dimensional quantum walks. *Communications in Computer and Information Science*, page 29–38, 2010. ISSN 1865-0937. doi: 10.1007/978-3-642-13861-4_3. URL http://dx.doi.org/10.1007/978-3-642-13861-4_3.

Benjamin Schumacher. Quantum coding. *Phys. Rev. A*, 51:2738–2747, Apr 1995. doi: 10.1103/PhysRevA.51.2738. URL https://link.aps.org/doi/10.1103/PhysRevA.51.2738.

Uwe Schöning. A probabilistic algorithm for k-sat and constraint satisfaction problems. *40th Annual Symposium on Foundations of Computer Science*, pages 410–, 1999.

Asif Shakeel. Efficient and scalable quantum walk algorithms via the quantum fourier transform. *Quantum Information Processing*, 19(9), Aug 2020. ISSN 1573-1332. doi: 10.1007/s11128-020-02834-y. URL http://dx.doi.org/10.1007/s11128-020-02834-y.

C. E. Shannon. A mathematical theory of communication. *The Bell System Technical Journal*, 27(3):379–423, 1948. doi: 10.1002/j.1538-7305.1948.tb01338.x.

V.V. Shende, S.S. Bullock, and I.L. Markov. Synthesis of quantum-logic circuits. *IEEE Transactions on Computer-Aided Design of Integrated Circuits and Systems*, 25(6):1000–1010, Jun 2006. ISSN 1937-4151. doi: 10.1109/tcad.2005.855930. URL http://dx.doi.org/10.1109/TCAD.2005.855930.

Neil Shenvi, Julia Kempe, and Birgitta Whaley. A quantum random walk search algorithm. *Physical Review A*, 67(5):052307, 2003.

Peter W. Shor. Algorithms for quantum computation: Discrete logarithms and factoring. *Proceedings 35th Annual Symposium on Foundations of Computer Science*, pages 124–134, 1994a.

P.W. Shor. Algorithms for quantum computation: discrete logarithms and factoring. *Proceedings 35th Annual Symposium on Foundations of Computer Science*, pages 124–134, 1994b. doi: 10.1109/SFCS.1994.365700.

Alexander Slepoy. Quantum gate decompostition algorithms. *Sandia National Laboratories*, 2006.

R. Solovay and V. Strassen. A fast monte-carlo test for primality. *SIAM Journal on Computing*, 6(1):84–85, 1977. doi: 10.1137/0206006. URL https://doi.org/10.1137/0206006.

Tommi Sottinen. Fractional brownian motion, random walks and binary market models. *Finance and Stochastics*, (5):343–355, 2001. doi: 10.1007/PL00013536.

Andrew Steane. Multiple-particle interference and quantum error correction. *Proceedings of the Royal Society of London. Series A: Mathematical, Physical and Engineering Sciences*, 452 (1954):2551–2577, 1996. doi: 10.1098/rspa.1996.0136. URL https://royalsocietypublishing.org/doi/abs/10.1098/rspa.1996.0136.

Mario Szegedy. Quantum speed-up of markov chain based algorithms. *45th Annual IEEE Symposium on Foundations of Computer Science*, 2004.

Alan Turing. On computable numbers, with an application to the entscheidungsproblem. *Proceedings of the London Mathematical Society*, s2-42(1):230–265, 1936.

Salvador Elías Venegas-Andraca. Quantum walks: a comprehensive review. *Quantum Information Processing*, 11(5):1015–1106, 2012.

J. von Neumann. First draft of a report on the edvac. *IEEE Annals of the History of Computing*, 15(4):27–75, 1993. doi: 10.1109/85.238389.

Stephen Wiesner. Conjugate coding. *SIGACT News*, 15(1):78–88, 1983. ISSN 0163-5700. doi: 10.1145/1008908.1008920. URL https://doi.org/10.1145/1008908.1008920.

Christof Zalka. Grover's quantum searching algorithm is optimal. *Physical Review A*, 60(4): 2746–2751, 1999.

A

MATHEMATICAL FOUNDATIONS

A.1 POSTULATES OF QUANTUM MECHANICS

Quantum mechanics, firstly discovered in the decade of 1920, is a mathematical framework for developing physical theories. In this section, the goal is to provide the basic postulates of quantum mechanics, which are formalized through Dirac notation. Further reading on this notation includes the work of Sakurai (1994) or *liboff*, and for an extensive review of quantum computation the book by Nielsen and Chuang (2011).

The first postulate defines where the processes of quantum mechanics take place. The *state* of a system describes it's physical characteristics, so some rules are required for these mathematical objects to have a connection to the real world.

Postulate 1 (State Space) *Any isolated physical system has an associated Hilbert Space, $\mathcal{H}$, known as the state space. The state of the system is wholly described by it's state vector $|\psi\rangle \in \mathcal{H}$. The physical system's degrees of freedom dictate the dimension of $\mathcal{H}$*

Note that this postulate does not tell us the Hilbert space of any given physical system, nor does it tell us it's state vector. It is generally hard to define the Hilbert space of an arbitrary system, which makes the work physicist have done developing certain theories, like quantum eletrodynamics, even more remarkable.

Considering the computational basis $\{|0\rangle, |1\rangle\}$, the simplest quantum system, the *qubit*, can be defined as

$$|\psi\rangle = \alpha |0\rangle + \beta |1\rangle , \tag{135}$$

where α, β are complex numbers and

$$|0\rangle = \begin{pmatrix} 1 \\ 0 \end{pmatrix} \quad \text{and} \quad |1\rangle = \begin{pmatrix} 0 \\ 1 \end{pmatrix} . \tag{136}$$

Because Hilbert spaces are also vector spaces, linear combinations of these states are also allowed

$$|\psi\rangle = \sum_i \alpha_i |\varphi_i\rangle . \tag{137}$$

Since $|\psi\rangle$ is required to be a unit vector, $|\psi\rangle\langle\psi| = 1$ or, equivalently,

$$\sum_j |\alpha_j|^2 = 1. \tag{138}$$

These combinations are the main difference between a classical bit and a qubit, known as *superpositions*, in which the states are not in a definite value before measurement. This is a well studied quantum phenomenon that leads to constructive and destructive interference between states, which is an aspect of quantum computation many algorithms exploit.

The second postulate aims to describe how a quantum system evolves with time, and it can be formulated in the following way.

Postulate 2 (Evolution) *The time evolution of a closed quantum system is described by a unitary operator. Considering an initial condition $|\psi_0\rangle$, then for any time evolution of a closed quantum system, a unitary operator U exists such that $|\psi_f\rangle = U|\psi_0\rangle$.*

Just as the first postulate does not specify a Hilbert space, the evolution postulate does not state which unitary operators U describe an arbitrary physical system. What it does state is that the evolution of a closed quantum system follows those rules. More specifically, the second postulate describes the dynamics of such systems. In the case of a qubit, any U can be performed in a realistic system as long as $UU^\dagger = U^\dagger U = I$, which is another way of saying that U is unitary.

There are a few unitary operators very relevant to quantum computation, known as *Pauli matrices*, that are usually composed to create more general matrices. These are defined as

$$I = \begin{pmatrix} 1 & 0 \\ 0 & 1 \end{pmatrix}, \quad X = \begin{pmatrix} 0 & 1 \\ 1 & 0 \end{pmatrix}, \quad Y = \begin{pmatrix} 0 & -i \\ i & 0 \end{pmatrix} \quad \textit{and} \quad Z = \begin{pmatrix} 1 & 0 \\ 0 & -1 \end{pmatrix}. \tag{139}$$

Postulate 2 tells us the relationship between the states of the system at two different times. An improved version of this postulate takes time as a continuous variable, stating that the temporal evolution of a closed quantum system can be described by the Schrodinger equation

$$i\hbar \frac{d|\psi\rangle}{dt} = H|\psi\rangle, \tag{140}$$

where $\hbar$ is the *Planck's constant* and H is a hermitian operator known as the *Hamiltonian* of the system. In principle, the Hamiltonian can be used to describe a system in it's entirety, however figuring out the Hamiltonian is generally a hard task.

So far only single quantum systems have been considered. The next postulate describes how one can create composite quantum systems made of smaller distinct systems.

Postulate 3 (Composite Systems) *The state space of a system composed of smaller sub-systems can be described by the tensor product of the individual state spaces $\mathcal{H}_1 \otimes \mathcal{H}_2$. Moreover, if the first system's state is $|\psi_1\rangle$ and the second is $|\psi_2\rangle$ then the state of the composite system is $|\psi_1\rangle \otimes |\psi_2\rangle$.*

The tensor product is used because of the nature of superposition in quantum mechanics. A system composed of subsystems $\{|\psi\rangle, |\varphi\rangle\}$ can be denoted as $|psi\rangle \otimes |\varphi\rangle$. Applying the superposition principle, that tells us that any complex linear combination of states belonging to the system should also be allowed, the tensor product naturally follows.

The tensor notation can be written in a more compact way. Considering a system described by n component states

$$|\psi\rangle = |\psi_0\rangle \otimes |\psi_1\rangle \otimes \cdots \otimes |\psi_{n-1}\rangle, \tag{141}$$

it can be rewritten as

$$|\psi\rangle = |\psi_0\rangle |\psi_1\rangle \cdots |\psi_{n-1}\rangle, \tag{142}$$

and even further compacted to

$$|\psi\rangle = |\psi_0\psi_1 \cdots \psi_{n-1}\rangle. \tag{143}$$

However, not all composite systems can be described as the tensor product of the component states. For example, state

$$|\psi\rangle = \frac{|00\rangle + |11\rangle}{\sqrt{2}}, \tag{144}$$

cannot be broken down further. These subsytems are known to be *entangled*, and the state in equation 144 is called a *Bell* state. Bell states describe the set of 2 qubit states that present maximum entangled, and are used in many quantum aplications like *quantum teleportation* and *superdense coding*.

As was aforementioned, closed quantum systems evolve unitarily in time. However, in order to do something useful with such a system, one must extract the classical information relating to the state of the system. This is achieved by the process of measurement, which imples some form of interaction with the system, thus making it no longer closed nor described by a unitary evolution.

Postulate 4 (Measurement) *Quantum measurements are described by a set, $\{M_m\}$, of measurement operators that act on the state space of the system, satisfying the completeness relation $\sum_m M_m^\dagger M_m = I$, where m referes to the measurement outcomes of the experiment. Considering a system with state $|\psi\rangle$, immediately before measurement, then the probability of event m is*

$$p(m) = \langle\psi| M_m^\dagger M_m |\psi\rangle. \tag{145}$$

The state of the system after the measurement will be

$$|\psi'\rangle = \frac{1}{\sqrt{p(m)}} M_m |\psi\rangle. \tag{146}$$

Measurement can be done and interpreted in several different ways, however this section focuses on what is called *projective* measurement. A projective measurement is described by an Hermitian operator, M, known as an *observable*, with spectral decomposition

$$M = \sum_m m P_m \tag{147}$$

where P_m is an Hermitian projection operator with eigenvalue m. For example, P_1 and P_2 are projection operators that are orthogonal to each other and whose product is a zero matrix. A set of operators with these characteristics obey the completeness equation

$$\sum_i P_i = I. \tag{148}$$

The probability of outcome m associated with the measurement of state $|\psi\rangle$ can be written as

$$p(m) = \langle\psi| P_m |\psi\rangle, \tag{149}$$

and knowing that m was the result of the measurement, the state of the quantum system is then

$$\frac{P_m}{\sqrt{p(m)}} |\psi\rangle. \tag{150}$$

An important case of projective measurement is when it is performed in the *computational basis* of a qubit. Given operators

$$M_0 = |0\rangle\langle 0| = \begin{pmatrix} 1 & 0 \\ 0 & 0 \end{pmatrix} \text{ and } M_1 = |0\rangle\langle 0| = \begin{pmatrix} 0 & 0 \\ 0 & 1 \end{pmatrix}, \tag{151}$$

it is obvious that they are Hermitian and that they obey the completeness relation. Consider again the state $|\psi\rangle = \alpha|0\rangle + \beta|1\rangle$. The probability of outcome 0 will be

$$p(0) = \langle\psi| M_0^\dagger M_0 |\psi\rangle = \langle\psi| M_0 |\psi\rangle = |\alpha|^2 \tag{152}$$

and outcome 1

$$p(0) = \langle\psi| M_0^\dagger M_0 |\psi\rangle = \langle\psi| M_0 |\psi\rangle = |\beta|^2. \tag{153}$$

For each of the outcomes, the state after measurement will be

$$\frac{M_0}{|\alpha|} |\psi\rangle = \frac{\alpha}{|\alpha|} |0\rangle, \tag{154}$$

$$\frac{M_1}{|\beta|} |\psi\rangle = \frac{\beta}{|\beta|} |1\rangle. \tag{155}$$

Projective measurement, in some ways, destroys the superposition of possible states. This is known as the *collapse of the wave function*.

B

CIRCUITS

B.1 QUANTUM FOURIER TRANSFORM

As was seen in section **??**, quantum computers can perform certain tasks more efficiently than classical computers. Another such example is the problem of finding the prime factorization of an n-bit integer, which the most efficient solution to date, proposed by Pollard et al. (1994), requires $e^{O(n^{\frac{1}{3}}\log^{\frac{2}{3}} n)}$ operations. In contrast, a quantum algorithm proposed by Shor (1994b) accomplishes the same task in $O((\log n)^2(\log\log n)(\log\log\log n))$ operations, which is an exponential gain due to the efficiency of the quantum Fourier transform.

The quantum Fourier transform is an implementation of the discrete Fourier transform over amplitudes of quantum states. It offers no speed ups when used in computing Fourier transforms of classical data, since the amplitudes cannot be accessed directly by measurement. Moreover, there is no known generalized efficient way of preparing the initial state to be Fourier Transform. What this means is that the uses of the QFT are not in the straightforward way of calculating discrete Fourier transforms, but in the form of algorithms, such as *phase estimation*, that take advantage of it's properties. This transform can be described as the following operation over an orthonormal basis $|0\rangle, |1\rangle, \cdots, |N-1\rangle$

$$QFT(|j\rangle) = \frac{1}{\sqrt{N}} \sum_{k=0}^{N-1} e^{\frac{2\pi ijk}{N}} |k\rangle, \tag{156}$$

where $N = 2^n$. With a little bit of algebra, this can be rewritten as a product

$$\begin{aligned} \frac{1}{\sqrt{N}} \sum_{k=0}^{N-1} e^{\frac{2\pi ijk}{2^n}} |k\rangle &= \frac{1}{\sqrt{N}} \sum_{k_1=0}^{1} \cdots \sum_{k_n=0}^{1} e^{2\pi ij(\sum_{l=1}^{n} k_l 2^{-l})} |k_1 \cdots k_n\rangle \\ &= \frac{1}{\sqrt{N}} \bigotimes_{l=1}^{n} (\sum_{k_l=0}^{1} e^{2\pi ijk_l 2^{-l}} |k_l\rangle) \\ &= \frac{1}{\sqrt{N}} \bigotimes_{l=1}^{n} (|0\rangle + e^{2\pi ij2^{-l}} |1\rangle) \end{aligned} \tag{157}$$

The quantum Fourier transform applied to a state as in equation 156 can then be rewritten as

$$QFT(|x_1,...x_n\rangle) = \frac{(|0\rangle + e^{2\pi i 0.x_n}|1\rangle)(|0\rangle + e^{2\pi i 0.x_{n-1}x_n}|1\rangle)\cdots(|0\rangle + e^{2\pi i 0.x_1x_2\cdots x_n}|1\rangle)}{2^{\frac{N}{2}}}, \quad (158)$$

where $x = x_1 2^{n-1} + x_2 2^{n-2} + \cdots + x_n 2^0$ and the notation $0.x_1 x_{l+1}\cdots x_n$ represents the binary fraction $\frac{x_l}{2^{i0}} + \frac{x_{l+1}}{2^1}\cdots\frac{x_m}{2^{m-l+1}}$. This is a very useful representation because it makes constructing an efficient circuit much simpler, as can be seen in figure 56. However, the circuit implementation of the QFT requires exponentially smaller phase-shift gates as the number of qubits increases. This can be somewhat mitigated by eliminating the smaller phase-shitft gates at the cost of some accuracy, as was shown in Coppersmith (2002) where he defined the *approximate* quantum Fourier transform. This approximation requires only $O(n \log n)$ gates, and work by Barenco et al. (1996) and Cheung (2004) established lower bounds for the probability of the approximate state accurately representing the state without approximation.

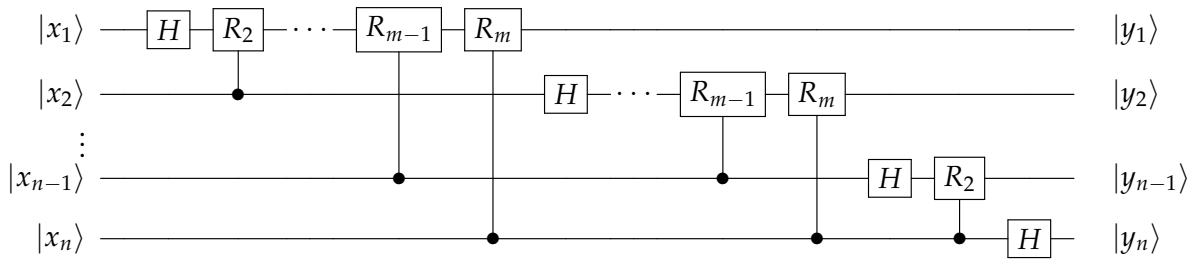

Figure 56: Temp

The rotation R_k in figure 56 is defined as the controlled version of

$$R_k = \begin{pmatrix} 1 & 0 \\ 0 & e^{\frac{2\pi i}{2^k}} \end{pmatrix}. \quad (159)$$

To verify that this circuit is the QFT, consider the state $|x_1\cdots x_n\rangle$ as input. Applying the Hadamard gate on the first qubit produces the state

$$H|x_1\cdots x_n\rangle = \frac{1}{\sqrt{N}}(|0\rangle + e^{2\pi i 0.x_1}|1\rangle)|x_1\ldots x_n\rangle. \quad (160)$$

The next operation is the rotation R_2, controlled by the second qubit, resulting in state

$$\frac{1}{\sqrt{N}}(|0\rangle + e^{2\pi i 0.x_1x_2}|1\rangle)|x_1\ldots x_n\rangle. \quad (161)$$

Applying the succesive rotations up to R_n appends an extra bit to the phase of the first $|1\rangle$, ultimately becoming

$$\frac{1}{\sqrt{N}}(|0\rangle + e^{2\pi i 0.x_1 x_2 \cdots x_n}|1\rangle)\,|x_1 \ldots x_n\rangle\,. \tag{162}$$

A similar process is applied to the second qubit, and at the end of the rotations the state is

$$\frac{1}{\sqrt{N}}(|0\rangle + e^{2\pi i 0.x_1 x_2 \cdots x_n}|1\rangle)(|0\rangle + e^{2\pi i 0.x_2 \cdots x_n}|1\rangle)\,|x_1 \ldots x_n\rangle\,, \tag{163}$$

and the successive application of this process to the remaining qubits results in state

$$\frac{1}{\sqrt{N}}(|0\rangle + e^{2\pi i 0.x_1 x_2 \cdots x_n}|1\rangle)(|0\rangle + e^{2\pi i 0.x_2 \cdots x_n}|1\rangle)\cdots(|0\rangle + e^{2\pi i 0.x_n}|1\rangle)\,|x_1 \ldots x_n\rangle\,, \tag{164}$$

confirming that this is indeed the Fourier transform derived in equation 158 minus the order of the qubits, which is reversed. It also shows that the QFT is unitary, since all operations in the circuit are unitary.

Counting the number of gates on the circuit, one can conclude that the first qubit will have 1 Hadamard gate followed by $n-1$ controlled rotations. The second qubit is another Hadamard followed by $n-2$ controlled rotations. After n qubits, the total number of gates will be $\frac{n(n+1)}{2}$. This means the circuit provides a $O(n^2)$ algorithm, compared to the fastest classical algorithm, the *Fast Fourier Transform* which requires $O(n2^n)$ operations. This is an exponential gain, which can be improved upon at the cost of accuracy, but it's not a replacement for calculating classical Fourier transforms for the aforementioned reasons.

B.2 MULTI-CONTROLLED NOT GATE

In order to run this circuit on a real quantum computer using Qiskit, one must first find a way of creating generalized CNOT gates, since it is not available in the base package. One approach to this problem is to decompose an arbitrarily controlled CNOT gate into elementary gates, as was done by Barenco et al. (1995). In this context, the main idea is that for any unitary operator U, there exists operators such that

$$U = \phi AXBXC, \tag{165}$$

where $ABC = I$, X is the Pauli-X and ϕ is a phase operator described by $\phi = e^{i\delta} \times I$.

In order to understand this method, a good first example is the Toffoli gate, as is shown in figure 57. The first rotation in the circuit is defined by the R_z matrix

$$R_z(\theta) = \begin{pmatrix} e^{i\frac{\phi}{2}} & 0 \\ 0 & e^{i\frac{\phi}{2}} \end{pmatrix}, \tag{166}$$

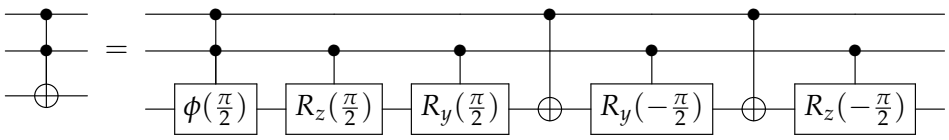

Figure 57: Toffoli decomposition

where $\theta = \frac{\pi}{2}$. Secondly, the R_y rotation is

$$R_y(\phi) = \begin{pmatrix} cos(\frac{\theta}{2}) & -sin(\frac{\theta}{2}) \\ sin(\frac{\theta}{2}) & cos(\frac{\theta}{2}) \end{pmatrix}, \tag{167}$$

and $\phi = \frac{\pi}{2}$. The following rotations are simply $R_z^\dagger$ and $R_y^\dagger$. Lastly, the phase operator ϕ is

$$\phi(\delta) = \begin{pmatrix} e^{i\delta} & 0 \\ 0 & e^{i\delta} \end{pmatrix} \tag{168}$$

where $\delta = -\frac{\pi}{2}$. This phase correction is considered because otherwise

$$R_z(\frac{\pi}{2})R_y(\frac{\pi}{2})XR_y(-\frac{\pi}{2})XR_z(-\frac{\pi}{2}) = \begin{pmatrix} 0 & -i \\ -i & 0 \end{pmatrix} \neq X. \tag{169}$$

Introducing the phase correction results in

$$\phi(\frac{\pi}{2}) \begin{pmatrix} 0 & -i \\ -i & 0 \end{pmatrix} = \begin{pmatrix} i & 0 \\ 0 & i \end{pmatrix} \begin{pmatrix} 0 & -i \\ -i & 0 \end{pmatrix} = \begin{pmatrix} 0 & 1 \\ 1 & 0 \end{pmatrix} = X \tag{170}$$

However, since this is a global phase, it won't be included since it has no effect on the result of the measurement.

A more generalized version of this method can be seen in figure 58. Each individual generalized CNOT gate in this circuit can be expanded as was done for the Toffoli gate example, stopping once the generalised inverter gates are simply Toffoli gates.

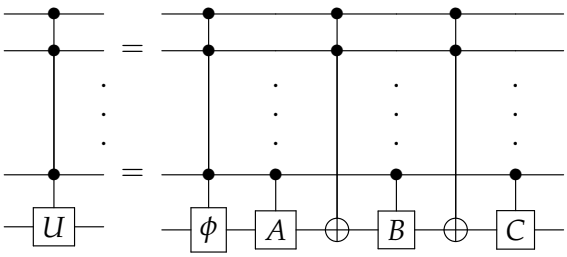

Figure 58: General decomposition

This was the chosen method because it provides a way of implementing arbitrarily controlled CNOT gates without the use of ancillary qubits, which are a scarce resource.